HTPO

ATCZ167

D.T1.3.2

ENG ASSESSMENT OF SEISMOGENIC POTENTIAL IN THE SURROUNDINGS OF LAA A.D. THAYA / PASOHLÁVKY AREA

December 2021

Co-financed by the European Regional Development Fund

Authors from the HTPO project team:	
Petr Špaček	Masaryk University
Jana Pazdírková	Masaryk University
Hana Krumlová	Masaryk University
Pavel Zacherle	Masaryk University
Fee-Alexandra Rodler	Zentralanstalt für Meteorologie und Geodynamik
Christa Hammerl	Zentralanstalt für Meteorologie und Geodynamik
Maria Papi-Isaba	Zentralanstalt für Meteorologie und Geodynamik
Wolfgang Lenhardt	Zentralanstalt für Meteorologie und Geodynamik
Rita Meurers	Zentralanstalt für Meteorologie und Geodynamik
Kontakt: spacek@ipe.muni.cz ; christa.hammerl@zamg.ac.at	

More information and other outputs on the project "HTPO – Hydrothermal potential of the area" Laa an der Thaya-Pasohlávky" can be found at:
https://www.at-cz.eu/cz/ibox/po-2-zivotni-prostredi-a-zdroje/atcz167_htpo

EUROPEAN UNION

Spolufinancováno Evropským fondem pro regionální rozvoj

Contents

1 Introduction

As a result of generally high stresses, the Earth's crust is often in a state close to brittle failure. Alterations of pore pressure in rocks, especially those that are rapid, lead to disturbances in the local stress-strength balance and can lead to stress relaxation through fracturing, generating earthquakes. Examples are known from all over the world, and the occurrence of artificially induced earthquakes in connection with the use of geothermal energy is not rare. In most cases, fracturing (both intentional for enhancing permeability and unintentional) is the result of rapid injection, but earthquakes can also be triggered by water extraction. Too large and rapid deformation due to increased pore pressure is surely undesirable from a technical and operational point of view. In the case of stronger induced seismicity in areas with a lack of public awareness and support, public pressure may make it very difficult to continue the heat mining project, possibly leading to its closure.

The induced earthquakes are, in principle, just like any other earthquake and cannot be distinguished from natural ones on the basis of their physical characteristics. The rate of induced seismicity is thus determined as that part of the total seismicity that is above the natural background level. Therefore, before commencing operations involving significant water handling at greater depths, it is advisable to first determine what the local natural seismicity rate is and to which structures in the Earth's crust the natural earthquakes are related. One of the important tasks of detailed seismological monitoring of the area is therefore to establish a baseline reference for future comparisons of seismicity before and after artificial intervention.

Since there may not have been any recent earthquakes directly in the low-seismicity area of interest, it is useful to monitor the level of seismicity in the wider region and also in the deeper past. Therefore, the wider Laa-Pasohlávky area up to 120 km away was chosen as the region of interest for seismological investigations. Regional scale knowledge is then used to understand the processes that can be expected at the local scale.

In this report, we briefly describe how we have been studying historical and present-day seismic activity in the wider region as part of a cross-border collaboration and what are the main features of the observed natural seismicity (Section 2), what the geological record has to say about pre-historical seismicity (Section 3), how we process the above observations into a baseline reference (Section 4), how are the earthquake-released seismic waves attenuated with distance (Section 5), and what strength of ground motions can be expected in case of stronger induced earthquake (Section 6).

2 Earthquake catalogues

Earthquake catalogues provide the basic comprehensive source of data used in earthquake science and seismic hazard. Catalogues prepared in this project are published as independent reports T1.2.1 (Hammerl et al., 2021) and T1.3.1 (Rodler et al., 2021). The paragraphs below relate directly to these reports and provide explanatory and supplementary information on them.

2.1 Historical Data and Macroseismic Earthquake Research

Christa Hammerl & Jana Pazdírková

2.1.1 Introduction

Within the framework of WP T.1.2 *Historical earthquake research and seismological description of the region Laa an der Thaya - Pasohlávky*, under WP T.1.2.1, earthquakes, starting with the year 1500, were investigated cross-border by the Institute of Physics of the Earth, Masaryk University (IPE) and by the Earthquake Service of the Central Institute for Meteorology and Geodynamics (ZAMG) and listed in the new earthquake catalogue for the project relevant region. The part discussed here deals with the catalogue from 1500 to 1999, since the methods used to compile the catalogue are fundamentally different from those used from 2000 onward.

A circle with a radius of 120 km and the centre of the circle between Laa an der Thaya/Austria and Pasohlávky/Czech Republic was defined as the project-relevant region (Fig. 1) in order to better describe the possible activity of individual faults and the effects of more distant earthquakes on the Laa an der Thaya/Pasohlávky region.

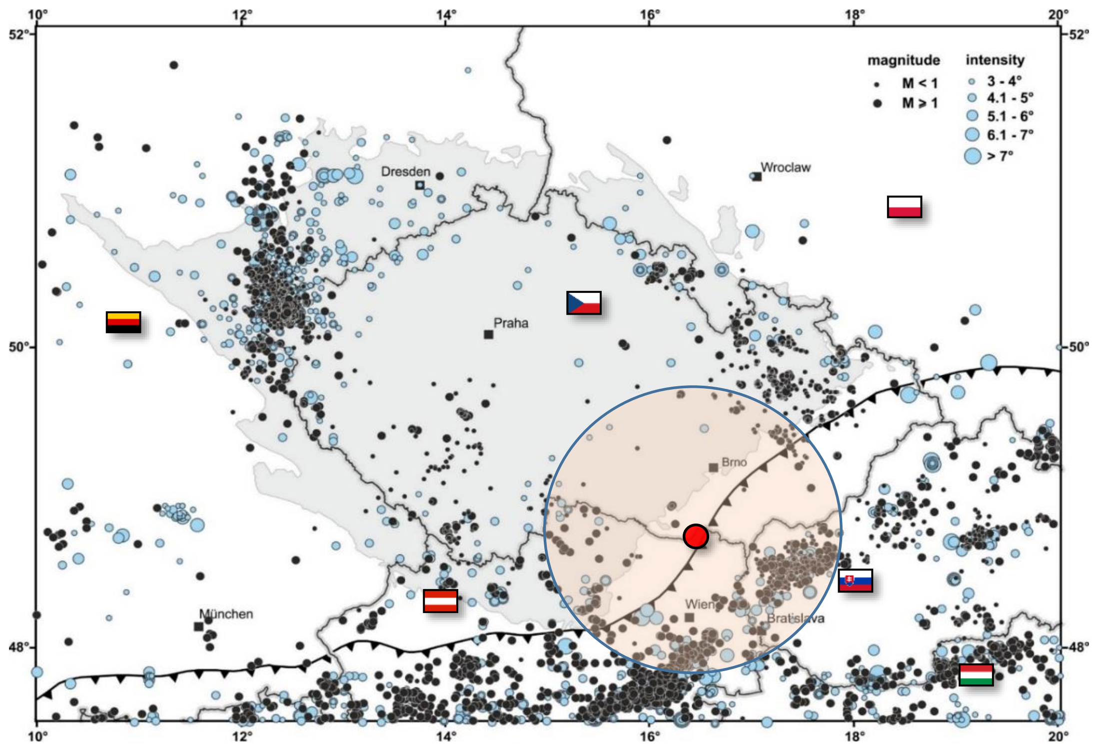

Figure 1. *Felt earthquakes for the period 1500-1999 and instrumentally measured earthquakes in the period 2000-2017. The circle has a radius of 120 km with the centre (red dot) between Laa an der Thaya/Austria and Pasohlávky/Czech Republic.*

The turning point in 2000 was chosen because, although there were already several seismic stations in the 20th century, their number did not increase significantly until the end of the millennium, and from that time onwards, above all, the exchange of station data between the various institutions started, which significantly increased the accuracy in the evaluation of the data and consequently in the parameter determination of the earthquakes.

The new aspect of WP T.1.2 within the HTPO project is that all known earthquakes from 1500 AD onwards were recorded and verified cross-border according to common methods in the study area. In order to fill gaps, new contemporary sources were additionally searched for. We chose the year 1500 as the beginning of the study period, because from this time on more reliable sources of information for the estimation of a historical earthquake can be expected in the archives.

2.1.2 Method

An essential aspect of reconstructing a historical earthquake is the need to use contemporary sources that are investigated in city archives, state archives, monastery archives, etc. These sources include annals, chronicles (Fig. 2a), accounts, damage assessments, diary entries, newspapers, and, especially in the 20th century, questionnaires (Fig. 2b) of earthquake services. Until the 18th century, these are mainly handwritten sources that are transcribed, translated, and documented.

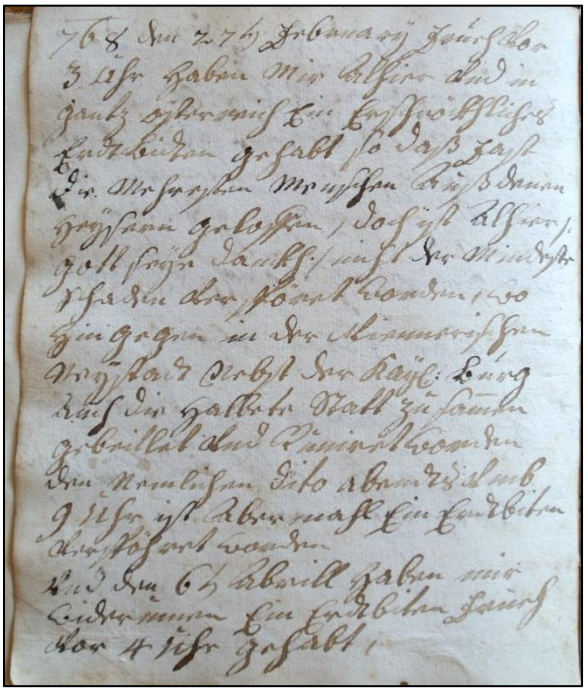

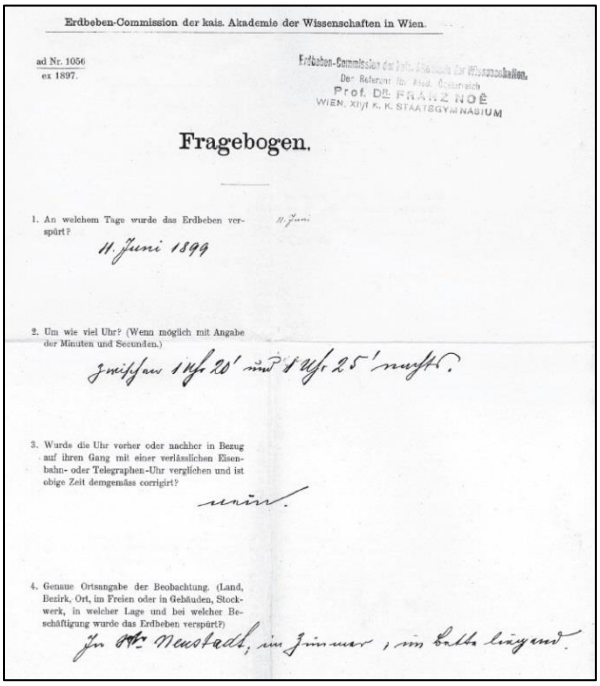

Erdbeben-Commission der kais. Akademie der Wissenschaften in Wien.

ad Nr. 1056
ex 1897.

Erdbeben-Commission der [illegible] Wissenschaften,
Der Referent für [illegible]
Prof. Dr. FRANZ NOË
WIEN, XIX/1 K. K. STAATSGYMNASIUM

Fragebogen.

1. An welchem Tage wurde das Erdbeben verspürt? 11. Juni

11. Juni 1899

2. Um wie viel Uhr? (Wenn möglich mit Angabe der Minuten und Secunden.)

zwischen 1 Uhr 20' und 1 Uhr 25' nachts.

3. Wurde die Uhr vorher oder nachher in Bezug auf ihren Gang mit einer verlässlichen Eisenbahn- oder Telegraphen-Uhr verglichen und ist obige Zeit demgemäss corrigirt?

nein.

4. Genaue Ortsangabe der Beobachtung. (Land, Bezirk, Ort, im Freien oder in Gebäuden, Stockwerk, in welcher Lage und bei welcher Beschäftigung wurde das Erdbeben verspürt?)

In Wr. Neustadt, im Zimmer, im Bette liegend.

Figure 2. a *(left) – Contemporary information about the earthquake of February 27, 1768 in the Gemein=Buch des guett Guettenbrun genandt. De Anno 1730. Source: Stadtarchiv Baden, MS GG/1.* ***b*** *(right) – Questionnaire of the Earthquake Commission of the Imperial Academy of Sciences in Vienna on the earthquake of June 11, 1899 in Ebreichsdorf, later administered by the Earthquake Service of ZAMG. The questionnaire was sent to Franz Noë, earthquake referent for Lower Austria. Source: ZAMG archive.*

Afterwards, a source-critical analysis is carried out; it is important to know who wrote the contemporary news about an earthquake, at which place and with which intention. Finally, the news are interpreted in context and with the knowledge of the respective zeitgeist.

This results in a number of so-called DPs/datapoints for each earthquake investigated, which are those locations where an earthquake was felt or caused damage. Coordinates are assigned to these DPs, for historical place names or place names that occur frequently, the correct interpretation is important. In the present project the cross-border cooperation was useful here.

If the significance of an earthquake message is sufficient, the DPs are assigned an intensity based on the EMS-98 – European Macroseismic Scale – in cooperation of IPE and ZAMG, one then speaks of IDPs/Intensity datapoints. By means of these IDPs the further parameters like epicentral intensity, focal depth and magnitude of an earthquake are determined. IDPs can also be used to create the "seismic history" of a site.

2.1.3 Strongest Earthquakes in the Region of Laa an der Thaya/Pasohlávky

In the project-relevant area, the strongest earthquake was a historical one, namely that of September 15, 1590, in Ried am Riederberg/Austria (Fig. 3). The epicentral intensity was 9° EMS-98, the magnitude (ML) was determined to be 5.8, and the focal depth was 6 km. The distance of the epicentre from Laa an der Thaya/Pasohlávky is about 70 km. Contemporary news around Laa an der Thaya/Pasohlávky are not available, although a local intensity of 5° EMS-98 (strong) would be plausible here.

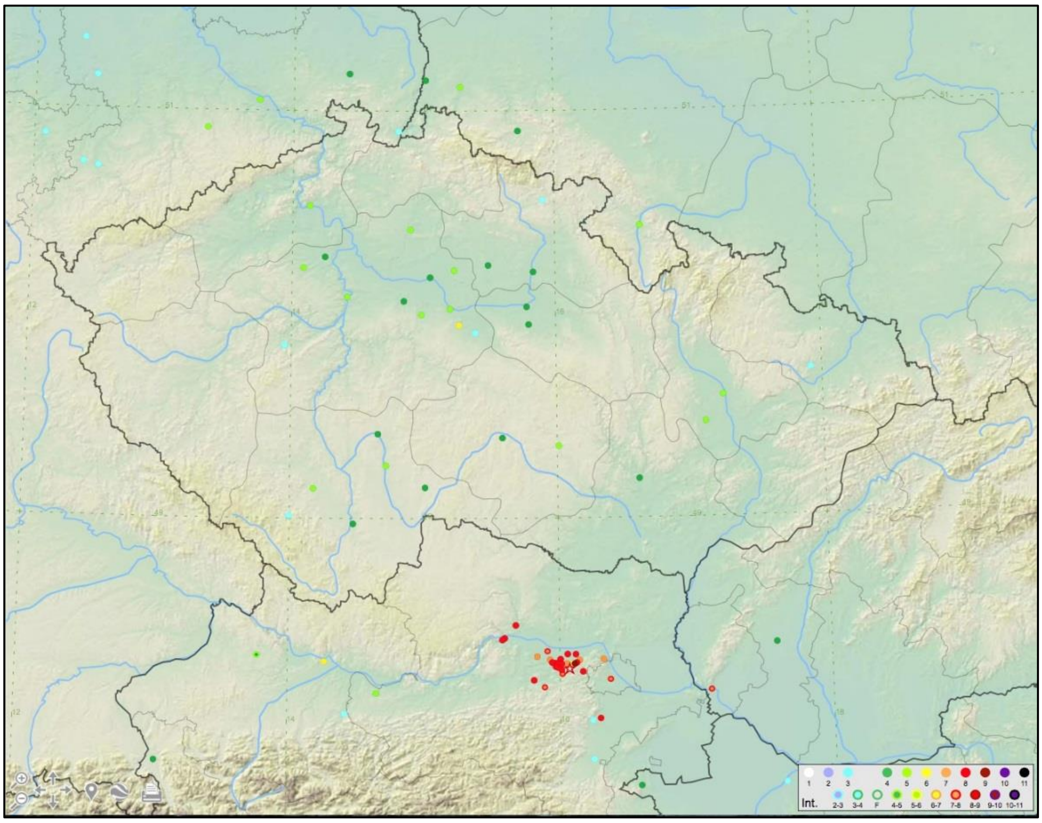

Figure 3. *Felt area of the earthquake of September 15, 1590. The damage area around the assumed epicenter in Ried am Riederberg is located west of Vienna.*

The second strongest historical earthquake in the project-relevant region on January 9, 1906, had its epicentre in Dobra Voda/Slovak Republic with an epicentral intensity of 8-9°, the magnitude (ML) was determined to be 5.7, and the focal depth was 9 km.

The epicentres of all damaging earthquakes ($I_0 \geq 6°$) within the circle (Fig. 1) were located on the Austrian and Slovakian territory.

The map (Fig. 1) also shows that the Austrian and Slovak part of the studied area is seismically more active than the Czech one, both in terms of number and intensity of earthquakes. In the immediate vicinity of the Laa an der Thaya/Pasohlávky area, no earthquake was recorded in the period 1500-1999. In the area up to 50 km from Laa an der Thaya/Pasohlávky only ten earthquakes with a maximum epicentral intensity of 4° EMS-98 occurred, the nearest of which, on April 18, 1912 with the epicentre 20 km from Laa an der Thaya/Pasohlávky, had an epicentral intensity of 4° EMS-98.

The epicentre of the earthquake of November 15, 1852 in Šaštín/Slovak Republic with an epicentral intensity of 6° EMS-98 and magnitude 4.3 was the closest of all damaging earthquakes to the project-centre Laa an der Thaya/Pasohlávky at a distance of 55 km.

The information on the earthquakes was obtained from the earthquake catalogues of ZAMG[1], IPE[2], SAV - Earth Science Institute, Slovak Academy of Sciences, Bratislava/Slovak Republic and GFÚ - Institute of Geophysics, AS CR, Prague/Czech Republic. We have revised the earthquakes with the focus on Czech and Austrian territory, the Slovak data were taken from the Slovak earthquake catalogue without revision.[3]

To assess the impact of strong earthquakes on the HTPO site, the 26 strongest earthquakes in the Austrian part of the study area were selected (Fig. 4 and Table 1). These were earthquakes with an epicentral intensity of ≥ 5-6° EMS-98, i.e., shaking that can cause damage to buildings. There were not such strong earthquakes in the Czech part of the study area and we do not have enough data (IDPs) for the Slovak earthquakes. For the selected earthquakes, a list of locations where the respective earthquake was felt or caused damage was prepared. Coordinates and intensities were assigned to the locations, which are referred to as IDPs. Figures 6 and 7 show the 26 strongest earthquakes listed in table 1 and their effects in an area up to 50 km from Laa an der Thaya/Pasohlávky. The map on the left (Fig. 4) shows the epicentres of these earthquakes, and the map on the right (Fig. 5) shows the IDPs of those earthquakes within a radius of 50 km around Laa an der Thaya/Pasohlávky. While the earthquakes closer to the project-relevant area reached a maximum intensity of 4° EMS-98 and did not cause any damage, strong earthquakes further away even caused minor damage in the form of fallen plaster or cracks in the plaster.

[1] AEC, 2021. Austrian Earthquake Catalogue. Computer file. Seismological Service of the Zentralanstalt für Meteorologie und Geodynamik (ZAMG), Vienna, Austria.

[2] Catalogue of Czech historical earthquakes, 2021. Computer file. Institute of Physics of the Earth (IPE), Masaryk University, Brno, Czech Republic.

[3] Labák P., 2001. Catalogue of macroseismically observed earthquakes on the territory of Slovakia since 1034 (version 2001, in Slovak). Geophys. Inst. Slov. Acad. Sci. Bratislava.

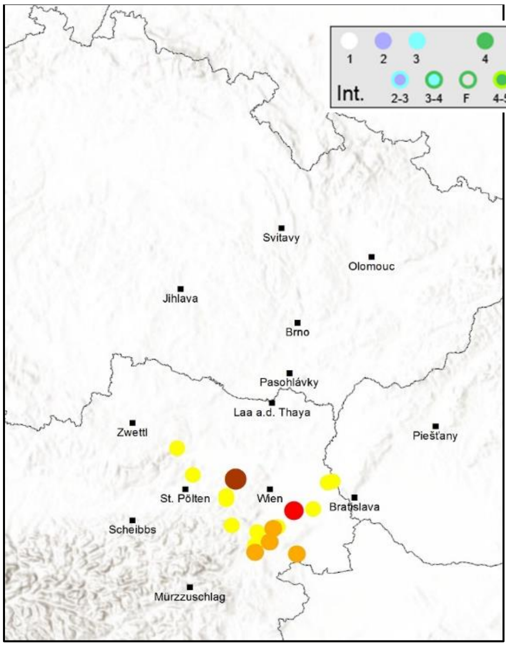

__Figure 4.__ Epicenters of the 26 strongest earthquakes in the Austrian part of the study area, listed in Table 1.

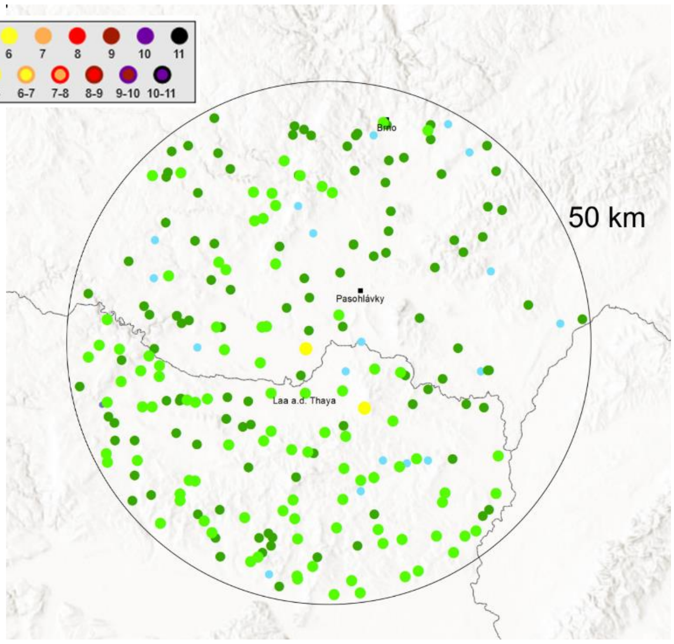

***Figure 5**. The map showing the IDPs of the 26 strongest earthquakes in the Austrian part of the study area within a radius of 50 km around Laa an der Thaya/Pasohlávky*

***Table 1.** 26 strongest earthquakes in the Austrian part of the study area Laa an der Thaya/Pasohlávky.*

	Year	mo	d	h	m	s	Lat	Long	z	*	M	*	I_0	Epicentre	Distance to „HTPO site“ (km)
1.	1590	9	15	23	50		48,26	16,07	6	*	5,75	*	9,0	Ried am Riederberg	68
2.	1590	9	15	17			48,26	16,07	6	*	5,20	*	8,0	Ried am Riederberg	68
3.	1927	10	8	19	49	0	48,07	16,58	6	*	5,20		8,0	Schwadorf	83
4 .	1938	11	8	3	12	0	47,96	16,40	10	*	5,00		7,0	Ebreichsdorf	95
5.	1768	2	27	1	45		47,82	16,24	9	*	5,00	*	7,0	Wiener Neustadt	112
6.	1766	8	5	5			47,81	16,61					7,0	Sankt Margarethen	113
7.	1766	8	16	21	7		47,81	16,61					7,0	Sankt Margarethen	113
8.	1963	12	2	6	49	0	47,88	16,37	8	*	4,50		6,5	Ebenfurth	104
9 .	1590	10	1				48,26	16,07	6				6,0	Ried am Riederberg	68
10.	1590	10	7	23			48,26	16,07	6				6,0	Ried am Riederberg	68
11.	1959	2	17	1	54	0	48,45	15,56	4	*	3,50		6,0	Senftenberg	77
12.	1590	6	29				48,14	15,99	12	*	4,50	*	6,0	Hochstrass	82
13.	1581	7	16	22	45		48,07	16,58	8	*	4,30	*	6,0	Schwadorf (?) od. 21.7.1581	83
14.	1953	5	2	12	37	0	48,08	16,75	8	*	4,10		6,0	Regelsbrunn	84
15.	1996	1	9	1	7	22	47,94	16,26	8	*	4,10		6,0	Ebreichsdorf	98
16.	1767	11	27	14			47,86	16,24					6,0	Theresienfeld	107
17.	1712	4	10				47,82	16,24	7	*	4,00	*	6,0	Wiener Neustadt	112
18.	1774	1	15	12	38		47,82	16,24	7	*	4,10	*	6,0	Wiener Neustadt	112
19.	1841	7	13	12	34		47,82	16,24	7	*	4,00	*	6,0	Wiener Neustadt	112
20.	1972	1	5	4	58	0	47,82	16,24	9		4,10		6,0	Wiener Neustadt	112
21.	1974	12	9	12	14	0	48,25	16,92	5		3,00		5,5	Marchegg	71
22.	1977	2	6	21	45	0	48,24	16,88	4		2,80		5,5	Breitensee/Marchfeld	71
23.	1873	1	3	18			48,16	15,99	10	*	4,00	*	5,5	Eichgraben	80
24.	1895	1	28	20	59		48,29	15,70	4	*	3,10	*	5,5	Herzogenburg	81
25.	1899	6	11		30		47,97	16,44	5	*	3,20	*	5,5	Ebreichsdorf	94
26.	1931	1	1	4	27	0	47,98	16,04	4	*	3,00	*	5,5	Weissenbach/Triesting	98

2.1.4 Résumé

The cooperation between IPE/MU and ZAMG on the common earthquake catalogue for the project region Laa an der Thaya/Pasohlávky resulted in 20 entries/earthquakes for the period 1500-1599 (parameters could not always be assigned), 6 entries/earthquakes for the period 1600-1699, 47 entries/earthquakes for the period 1700-1799, 148 entries/earthquakes for the period 1800-1899 and 440 entries/earthquakes for the period 1900-1999.

A good example of the importance of cross-border cooperation is the earthquake of November 8, 1938 in Ebreichsdorf. Fig. 6 shows for which locations information on this earthquake was available in the Austrian Earthquake Catalogue. By adding the IDPs from data from GFÚ Prague, a completely new picture of the far field of the earthquake emerges (Fig. 7).

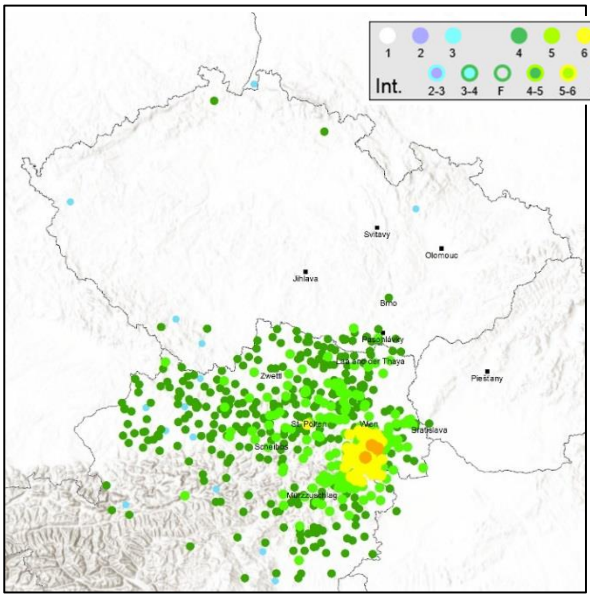

Figure 6. *IDPs of the November 8, 1938 earthquake, reproduced from the Austrian Earthquake Catalogue.*

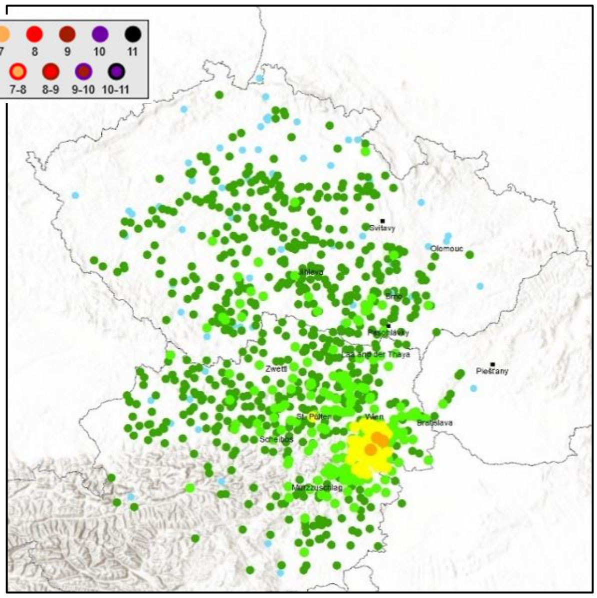

Figure 7. *IDPs of the earthquake of November 8, 1938, from the Austrian Earthquake Catalogue and from GFÚ Prague.*

For the following damaging earthquakes, cross-border cooperation significantly increased the number of IDPs: February 27, 1768 35 IDPs (A) plus 11 IDPs (CZ), October 8, 1927 602 IDPs (A) plus 52 IDPs (CZ), November 8, 1938 572 IDPs (A) plus 396 IDPs (CZ), December 2, 1963 408 IDPs (A) plus 331 IDPs (CZ).

It was found that cross-border cooperation using the same methods significantly improved the earthquake catalogue for the project-relevant region, contributing to a reliable assessment of the earthquake hazard in this area.

2.2 Instrumental Data and Harmonized Catalogue

Jana Pazdírková, Fee-Alexandra Rodler & Hana Krumlová

2.2.1 Monitoring network

The main goal of this part of the project was to collect relevant data concerning the instrumentally recorded earthquakes originated in the project region (Laa/Pasohlávky + 120 km radius). The Number and distribution of available seismic stations (Fig. 8) play a crucial role in the detection capability of a network and thus the identification of seismic events and their location.

Seismic stations began to be built in Central Europe at the beginning of the 20th century. However, they were few in number and could only register strong earthquakes. The number of stations started to increase in the second half of the 20th century, but it was only the digitization of stations in the last decade of the last century, that contributed to better monitoring of weak earthquakes.

In 1990, the stations VIE in Vienna (ZAMG) and ZST near Bratislava (SAS) existed within the study area and neither of them was suitable for recording weak earthquakes. Also, stations in the more distant vicinity of Laa-Pasohlávky contributed mainly to the location of strong felt earthquakes and could not be used to locate micro-earthquakes within the study area.

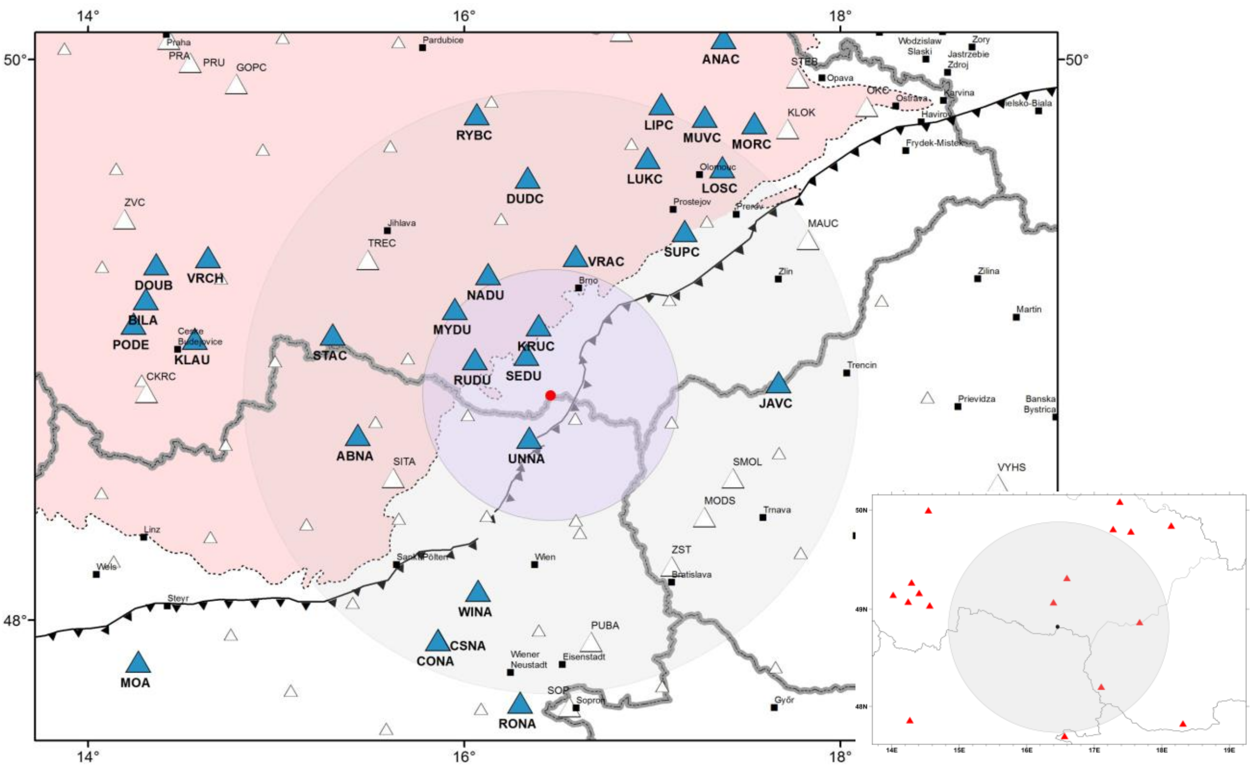

Figure 8: *Map of seismic stations operating in 2021. Small map on the bottom right shows the situation in 2000 for comparison.*

The situation began to improve during the 1990s, where more stations were added near and inside the region of interest. The seismic network around the Temelín NPP was put into operation by IPE in 1991 and the broadband station VRAC (IPE) was built near Brno in 1993 for CTBTO purposes. The station MORC was one of the first stations of the GEOFON project in 1994. Stations KRUC near Moravský Krumlov and JAVC near Velká Javorina (IPE) were built in 1995 and the station MOA near Molln in Upper Austria (ZAMG) was upgraded in 1996 in the frame of the joint ZAMG and IPE project

ACORN. More stations were added in the northern border area of the Czech Republic and in Slovakia. These modern digital stations were able to record even very weak local earthquakes. However, the location of these tremors was in some cases very imprecise, either because of the distribution of stations relative to the focus or because of the limited possibility of sharing data between institutions.

A turning point came in 2000, when the development of digital technologies enabled the exchange of larger data volumes between institutions. This greatly improved the geometry of virtual networks run by the individual institutions and allowed better detection and location of even very weak earthquakes. The year 2000 was therefore chosen as the initial year for the catalogue compilation.

In the following years, more seismic stations, both permanent and temporary, were added in and around the study area (Fig. 8). The most important ones for seismicity monitoring within the HTPO project are the station CONA (ZAMG), in service since 2006, the Dukovany local network (IPE) since 2014, the station SITA station in Lower Austria (TU Vienna) and the temporary stations of the AlpArray project on Austrian, Czech and Slovak territory. Following the launch of the HTPO project in 2018, the station UNNA (ZAMG) was built in the very centre of the study area. The newly established stations ABNA and WINA (ZAMG) as well as STAC and RYBC (IPE) allow for better location of the micro-earthquakes.

2.2.2 Discrimination of seismic events

Small-magnitude earthquakes play a major role in determining the magnitude distribution and occurrence rate, especially in stable continental regions, where seismicity is low. Therefore, data from seismic stations are subjected to very detailed manual analysis. This approach is necessary to avoid overlooking weak local tectonic events since, even with acceptable background noise, it is virtually impossible to set the automatic localization parameters to detect earthquakes below a certain magnitude. All detected seismic events are processed and evaluated by type (such as earthquake, induced event or explosion) resulting in a database table or catalogue of recorded earthquakes.

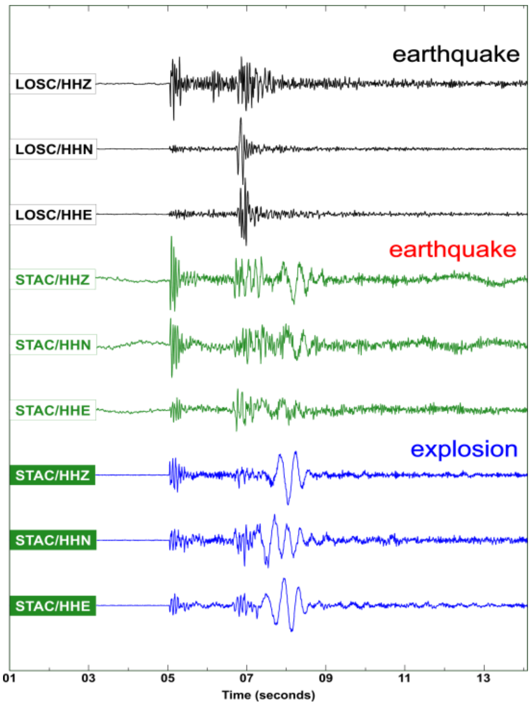

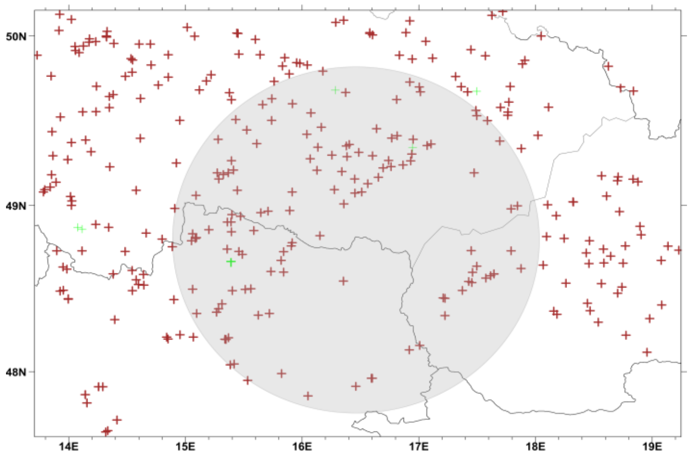

Figure 9: *Examples of seismic records of earthquakes versus a quarry blast (left). Because seismograms can look very similar, the knowledge of blasting points is very important, which is why we maintain a database of known active quarries (right).*

Since seismometers record all types of ground vibration, earthquake catalogues are contaminated by man-made events (mainly quarry blasts). Therefore, in order to determine the real seismicity of the region, it is necessary to discriminate quarry blast records or other man-made events from earthquake catalogues. Because seismograms can look very similar, this is not always an easy task. Seismic discrimination is usually performed by visually inspecting the records, calculating the event parameters, such as epicentre and magnitude, and checking the map for quarries near the epicentre location. Many quarries are well established and produce frequent explosions, that sometimes can be identified simply by their locations, which is why we maintain a database of known active quarries (Fig. 9). In case of doubt, we seek confirmation from local authorities (quarries, military training sites, construction companies, mayors, etc.) as to their possible origin. Events of dubious origin are conservatively considered as potential earthquakes, until they are proven to be otherwise. Also, the polarity of the first P-wave motion is always taken into account if it can be reliably determined.

2.2.3 Compilation of the instrumental catalogue

The data for compilation of the instrumental catalogue 2000-2017 has been adopted from all available sources to ensure the best coverage of the area of interest. These were mainly Austrian catalogues produced by ZAMG and Czech catalogues produced by the IPE, Masaryk University, Brno. We also collected data from the Institute of Geophysics of the Czech Academy of Sciences, the Slovak catalogues by the Slovak Academy of Sciences and the Hungarian catalogues by GeoRisk Ltd. All these catalogues were merged and the data was analysed in great detail. Suspicious events (possible explosions, mislocation) or incorrectly identified events were either newly located or excluded. The 18-year catalogue now consists of 2477 earthquakes.

The catalogue for the project monitoring period 2018-2021 was compiled continuously after each monitoring period in a similar way. Any suspicious phenomena were discussed as soon as possible after their detection. During this time period of less than 4 years, 1098 earthquakes have been recorded. Due to this detailed analysis it was possible to compile the most accurate catalogue of earthquakes originated in the study area, which does not contain any false earthquakes.

Our study showed, that on a small scale (area of 50 km radius) the area is seismically relatively quiet. Even the newly installed station UNNA did not enhance the number of detected small scale local earthquakes. During the monitoring period of the HTPO project from August 2018 to September 2021 no induced events connected to the extraction of fluids in Laa a. d. Thaya and Pasohlávky were detected and only 10 weak local earthquakes were registered.

In total, the instrumental catalogue for the time period 2000-2021 (Fig. 10) contains 3575 earthquakes with magnitudes ranging from -1.4 ML to 4.8 ML. The strongest event was the Ebreichsdorf earthquake south of Vienna on 11 July 2000 with a magnitude of 4.8. Only two very weak earthquakes of magnitude 0.0 and 0.2 were registered in the centre of the area of interest between Laa and Pasohlávky (Fig. 10).

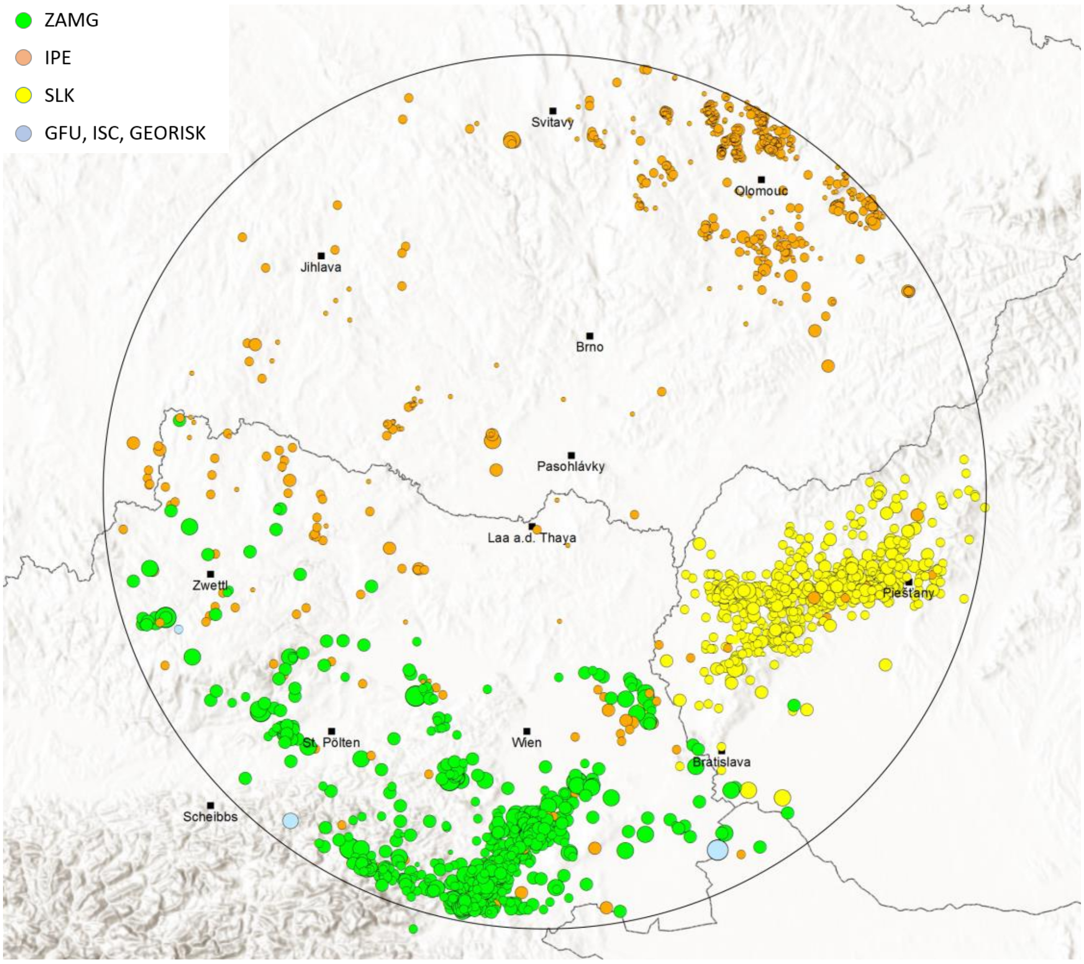

Figure 10: *Map of instrumentally recorded earthquakes in the compiled catalogue for the time period 2000-2021 containing 3575 earthquakes with -1.4 ≤ ML ≤ 4.8.*

2.2.4 Local Magnitude Homogenization

Before performing any scientific analysis, it is critical to assess the quality, consistency and homogeneity of the catalogue data. Therefore we compared the epicentre locations and magnitudes of earthquakes listed in both the Austrian and Czech catalogues. It turned out that the calculated epicentre locations are mostly very similar, however, higher discrepancies appeared, when comparing the local magnitudes.

The local magnitude ML ("Richter magnitude") is the most commonly used in the local and regional scales. It is based on measurement of the maximum ground motion displacement recorded by a seismograph. Since current stations measure velocity, not displacement, the maximum amplitude and period, determined with calibration curves, are used as inputs to displacement conversion formulas for ML calculation. Also, different institutions use different methodologies for reading the maximum amplitude and to calculate the network magnitude. The Institute of Physics of the Earth computes local magnitudes following equation [1] proposed by Scherbaum and Stoll 1983, which has been used since it was developed, leading to consistent results within time and for all stations of the Institute of Physics of the Earth networks.

$$M_L = log_{10}\left(\frac{u*2800}{0.6325}\right) + 1.4 * log_{10}(s) + 0.1 \qquad [1]$$

Here, *u* is the maximum displacement (amplitude) in mm and *s* the hypocentral distance in km. The amplitude is read on the vertical component of the velocity, obtaining the amplitude in nm and the period in seconds. The determination of the dominant frequency (or the period of the phase) is subjective and affects the resulting amplitude and thus the magnitude value. The ZAMG computes the magnitude from amplitude values of the north and east components. Before Spring 2004, local magnitude computation followed equation [2], where *R* is the epicentral distance in km, A the amplitude in nm and T is the period of the signal in seconds. Since spring 2004, local magnitudes are calculated with equation [3], where V is the maximum phase velocity in nm/s and Δ is the hypocentral distance in degrees.

$$M_L = log_{10}\left(\frac{A}{T}\right) + 2.2 * log_{10}(R) + 0.94 \qquad [2]$$

$$M_L = log_{10}(V) + 1.66 * log_{10}(\Delta) - 0.304 \qquad [3]$$

We conclude that the discrepancies found in ML values for common events mainly derive from the diverse methodologies to calculate the magnitude. The radiation characteristics of the environment may also play an important role, especially in this area at the contact of different geological units.

In order to define a homogeneous magnitude for the calibration of an Intensity Attenuation Model, we considered linear regression relations between ML pairs calculated by ZAMG and IPE (Fig. 11). We found the following magnitude relationships:

$$M_L^{ZAMG} = 0.86 * M_L^{IPE} + 0.54 \qquad [4]$$

$$M_L^{IPE} = 0.87 * M_L^{ZAMG} - 0.28 \qquad [5]$$

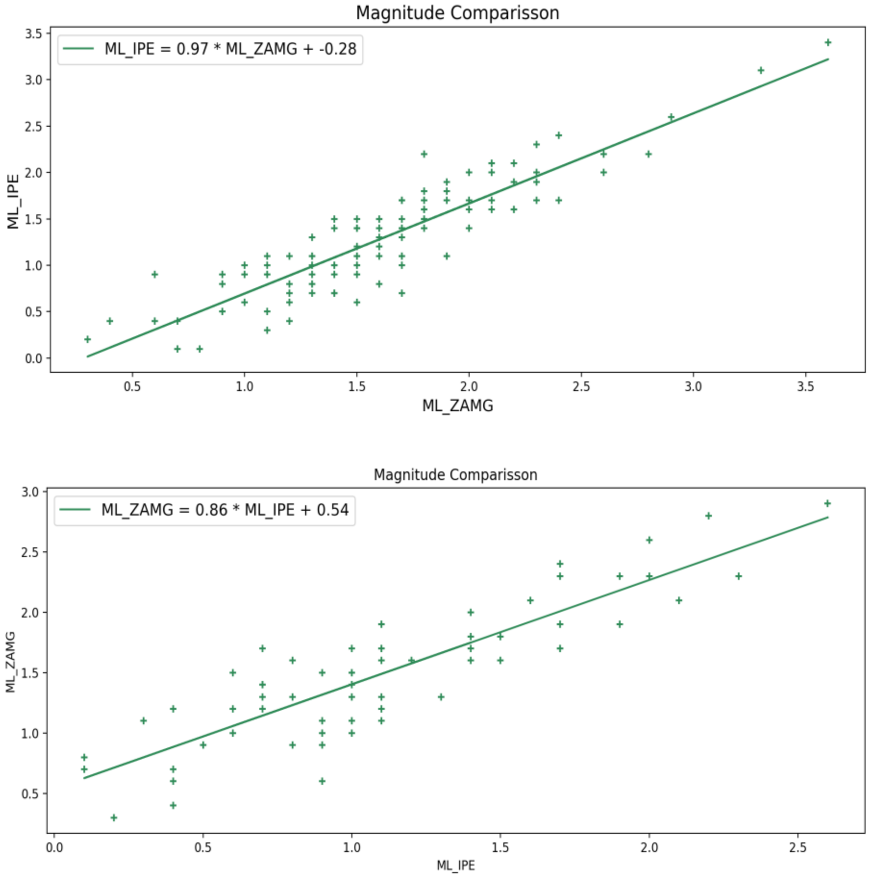

Figure 11: *Linear regression plots of ML pairs for ZAMG and IPE and corresponding conversion relations.*

2.2.5 Earthquake Detectability

Any earthquake catalogue is a result of signals recorded on a (spatially and temporally heterogeneous) network of seismometers and processed by humans using a variety of software and assumptions. The magnitude detection threshold of a seismic network is of great importance not only for the general operation of seismic observatories but also for the monitoring of induced seismicity. The detection capability of a network depends on many factors such as the density and distribution of seismic stations, their site conditions, their recording characteristics, and their data link to the processing centre. Thus, even the best earthquake catalogues are heterogeneous and inconsistent in space and time and the evaluation of catalogue completeness is by no means an easy task.

Different methods exist to calculate the detection capability of networks. One approach is, to calculate the magnitude of completeness Mc which is the minimum magnitude above which all earthquakes are reliably recorded (Section 2.2.6). Another approach is based on measured noise statistics and depends on the network geometry, the detection threshold at the individual stations and the minimum number N of station records required to reliably exclude false detections (Möllhoff et al., 2019). The detection threshold at individual stations is surpassed, once the signal-to-noise ratio (SNR) between maximum event amplitude A and noise amplitude d is larger than 3. Following the method of Möllhoff et al. (2019), the minimum detectable M_L is calculated for each point in a grid of hypothetical epicentres covering the network region of interest. The procedure is as follows:

1) Calculate the epicentral distances R [km] between the grid point and each station.

2) For a range of values, calculate for each station the maximum ground displacement amplitude A [nm/s] from the equation for the ML scale for Austria:

$$M_L = log_{10}(A) + 1.66 * log_{10}(R) - 0.37 \qquad [6]$$

3) Find the smallest ML value for which the condition A > 3 d is met for at least N stations.

To quantify the seismic background noise, we calculated power density functions (PDF) of power spectral densities (PSD) in the frequency domain with the PPSD routine in ObsPy (Krischer et al., 2015). Figure 5 shows a sample PDF of the vertical component data of station CONA, located northwest of Vienna (see station map in Fig. 13).

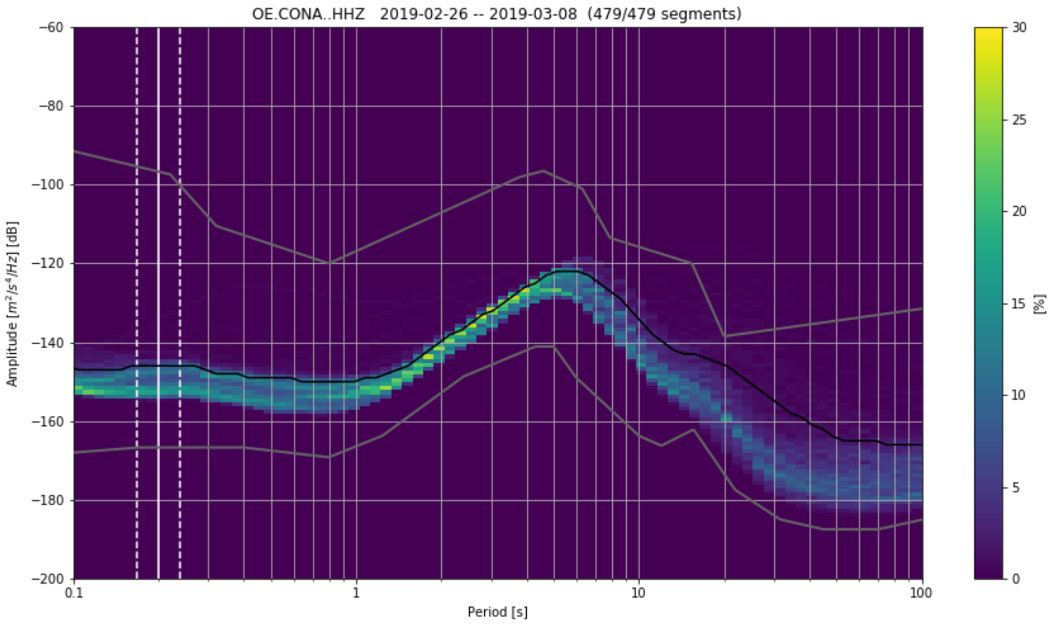

Figure 12: *Representation of power spectrum densities (PSD) as power density function (PDF) for vertical component data of station CONA for the time period 2019/02/16 to 2019/03/08. Also shown are the statistical quantities mode (black solid line) and the Peterson (1993) New High and Low Noise Models (grey solid lines).*

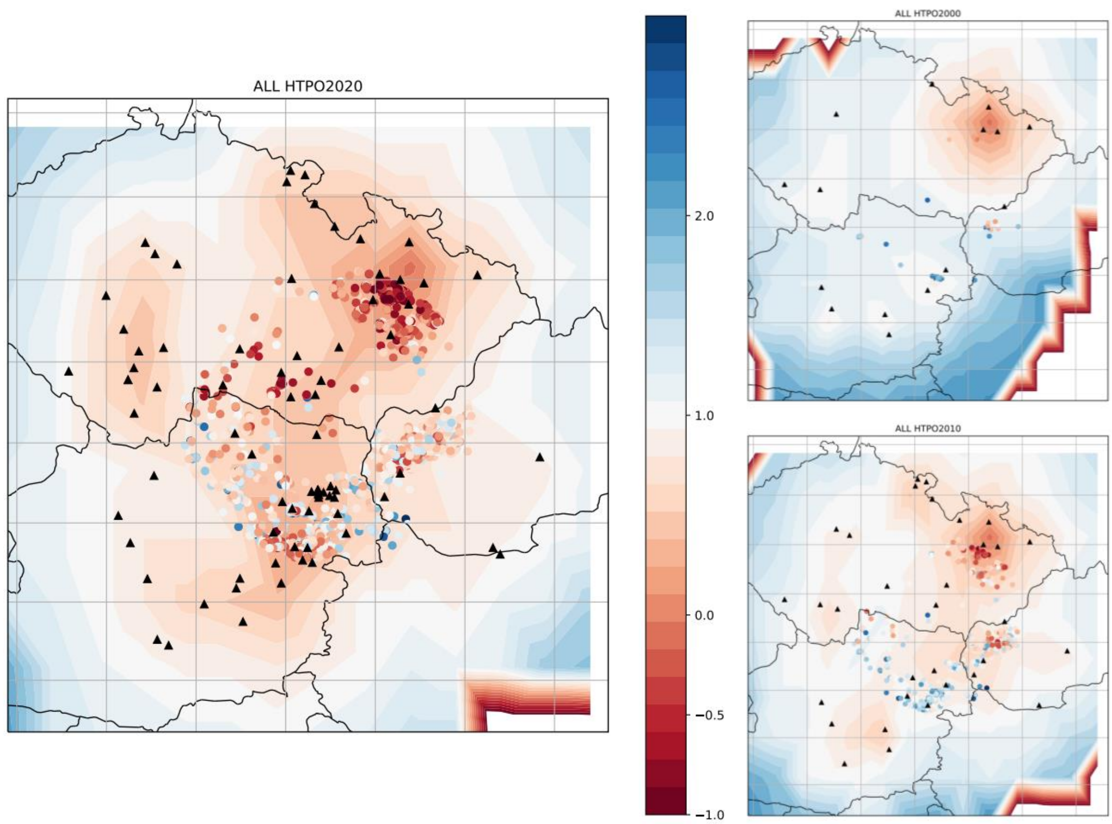

Figure 13: *Geographical distribution of the minimum detectable magnitude M_L for the border region SK-CZ-AT, based on measured P90 station noise levels and assuming event detection by at least four stations with SNR > 3. The figures demonstrate the improvement of event detectability due to the network enhancement, with the most recent one from 2020 (left) compared to the years 2000 (right-top) and 2010 (right-bottom).*

2.2.6 Catalogue Completeness and Magnitude-Frequency Distribution

The Magnitude of Completeness, M_C, is defined as the lowest magnitude at which 100% of the earthquakes in a space-time volume are detected (Rydelek and Sacks, 1989). Below M_C , a fraction of events is missed by the network, either because they are too small to be recorded on enough stations, or, in case of an aftershock sequence, because they are too small to be detected within the coda of larger events (Woessner and Wiemer, 2005). M_C is often estimated by fitting a simple power-law, the so called Gutenberg-Richter (GR) law, to the observed frequency-magnitude distribution (FMD). The FMD describes the occurrence rate for earthquakes of each considered magnitude (Ishimoto and Iida, 1939; Gutenberg and Richter, 1944):

$$log_{10}(N) = a - b * M \qquad [7]$$

where N is the total number of magnitudes larger or equal than M and a and b are coefficients. In this equation the a-value characterizes the seismic activity in the studies region and the b-value describes the relative size distribution. Especially the estimation of the b-value is critical to assessing the likelihood of an earthquake, so it plays an important role in hazard assessment studies. To estimate the b-value, we used a maximum-likelihood technique proposed by Aki (1965):

$$b = \frac{log_{10}(e)}{\overline{M} - \left(M_C - \frac{\Delta M}{2}\right)} \qquad [8]$$

where log (e) is a constant, M_C is the minimum magnitude of completeness, $\overline{M}$ is the mean magnitude of a sample of events with M ≥ M_C and M is the magnitude bin. Since a reliable M_C determination is vital for numerous hazard-related studies, we have used three different catalogue based methodologies (MAXC, EMR, GFT) presented by Mignan and Woessner (2012), to determine the completeness magnitude for the HTPO catalogue.

The Maximum Curvature (MAXC) technique consists of defining the point of the maximum curvature of the frequency-magnitude curve, which in practice matches the magnitude bin with the highest frequency of events in the non- cumulative FMD (Figure 14, left).

Another method proposed by Woessner and Wiemer (2005) is the Goodness-of-fit (GFT) method, that basically tries to fit the Gutenberg-Richter Model to the observed data. The entire magnitude range (EMR) method is the same as the GFT, but also includes events below Mc (Figure 14, right). The results for the historical and instrumental catalogue are shown in Table 2.

***Table 2:** Completeness Magnitude and Gutenberg-Richter a- and b-values for the historical and the instrumental HTPO catalogues.*

time period	No. of evens	Method	M_C	a	b
2000-2021	3573	EMR	0.5	3.55	0.61
2000-2021	3573	MAXC	0.6	3.47	0.56
2000-2021	3573	GFT	0.6	3.55	0.65
1581-1999	487	MAXC	2.6	3.57	0.51
1581-1999	487	EMR	2.6	4.83	0.9
1581-1999	487	GFT	2.7	3.79	0.58

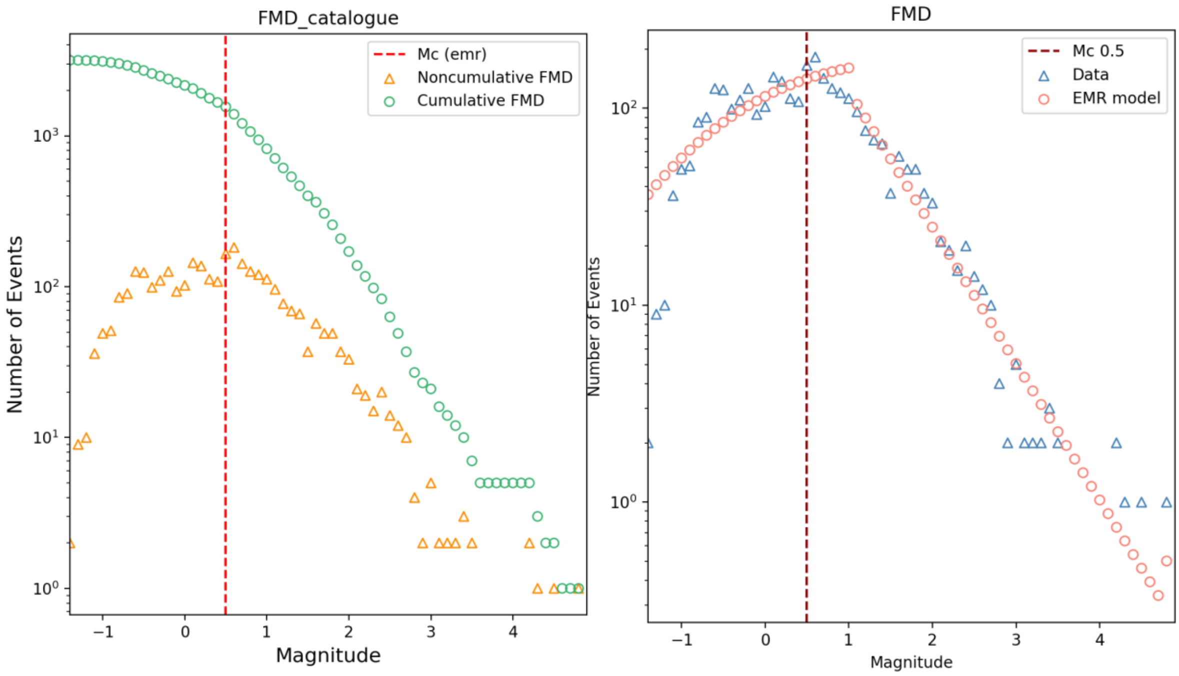

***Figure 14:** (left) FMD in cumulative and non-cumulative form and corresponding M_C estimates. (right) EMR technique - Maximum likelihood estimate of M_C for the subset of the 2000-2017 subset of the HTPO catalogue.*

3 Faults and paleoseismicity

Petr Špaček

Earthquakes, whether weak or strong, occur in most cases as a result of a sudden slip on a fault. Knowing the location and geometry of faults in the region of interest and understanding their young activity helps in assessing the probability and magnitude of future earthquakes. As with seismicity observations, it is important to know the context of the broader area of interest and to study faults on a regional scale. For this reason, we have also addressed faults in the context of this project, and we have included data from broader area. Faults that have been active over the last thousands and tens of thousands of years are of particular interest. We have analysed the fault network using main available geological, geomorphological and geophysical data with a focus on faults that are breaking the surface. Detailed investigations were carried out at selected localities near faults where sediment disturbance may provide a record of stronger prehistoric earthquakes or, conversely, their absence may rule out the possibility that one occurred. Below we give a brief overview of the results, including an example of research on an important regional fault in the eastern part of our area of interest and an example of structure that likely indicates a stronger paleoearthquake.

3.1 Fault network in Laa-Pasohlávky area

The conditions for fault mapping in the Laa-Pasohlávky area are unfavourable due to the prevailing lithology and flat relief. Faults are rare and apparently incomplete in geological maps of the area. The main faults and their indications, which we discuss briefly below, are shown in Fig. 15.

The most prominent fault structure is the frontal thrust of the Alpine-Carpathian fold-and-thrust belt in the eastern neighbourhood of the narrower area of interest. The youngest phases of thrusting are considered to be of Karpatian (Middle Miocene) age.

In the geological model of the project area (Nehyba et al. 2021), the dominant tectonic structure is a fault system with a general SSE-SSW trend and NW dip located in the axis of the area of interest, here called the Dyje fault system. These faults splay off from Mailberg fault – an important fault moderately dipping to SE, with normal slip leading to vertical throw of >2000 m during mid-Jurassic (Wagner 1998). As indicated in seismic reflection profiles SSW from the area of interest, extensional kinematics on this fault continued in Early Miocene then followed by a reverse slip phase in Karpatian and Badenian (Granado et al. 2016). The activity of the Dyje fault system in Tertiary is not well known. It does not have any distinct manifestations in the relief, but in the section Laa - Pasohlávky these faults may control the direction of flow of the river Dyje and some geologists considered them active in Quaternary (Zeman 1974). In the geological maps, several presumed faults at low angle to this fault system and to the frontal thrust are indicated in the wider area, but their position is very probably strongly inaccurate (and therefore they are not shown in Fig. 15).

A regionally significant Diendorf fault, which we have studied in more detail and is described below, runs less than 20 km west from Mailberg-Dyje fault system and generally parallel to it.

Other systems may be indirectly indicated by topographic relief. The regionally dominant is the system of WNW-ESE to NW-SE striking topolineaments parallel to the valleys of the rivers Dyje and Jevišovka. This is an extensive and penetrative system of short lineaments (edges, valleys and ridges) that may have been formed as a result of erosion of soft sediments (and saprolites) controlled by a system of faults or joints. In this direction, we also observe some discontinuous geophysical indications (gravity and magnetic fields, vertical electrical sounding and locally measured electrical resistivity tomography profiles). In the southeast of the area, on either side of the thrusting front, we observe a rather pronounced NNW-SSE topolineament system, which also corresponds to some gravity indications further north. Similarly oriented faults have been locally observed in Karpatian clays in a clay pit near Hevlín, north of Laa (Otáhalová and Melichar, 2007). Both the latter systems disrupt the course of the frontal thrust and can thus be considered partly active during and after the thrusting. The young activity of these systems has not yet been comprehensively assessed. However, different heights of fluvial accumulations have been interpreted as possible manifestations of active faulting in Middle to Late Pleistocene (e.g., Zeman in Dlabač et al. 1972).

Regional orientation of maximum horizontal stress, s_H, rotates significantly from NE-SW beneath the E Alps to NW-SE in the central and eastern Bohemian Massif. Local stress data are not available, but the regional model suggests a NNW-SSE (azimuth 150 to 180°) orientation of s_H in the area of interest. Thus, for the NNW-SSW and WNW-ESE fault systems we can expect more or less similar and relatively low slip potential. The NNW-SSE fault system may be significantly more optimal for slip. Large uncertainties in stress field (both orientation and shape of stress tensor) and fault dips unfortunately prevent a quantitative assessment of fault slip potential.

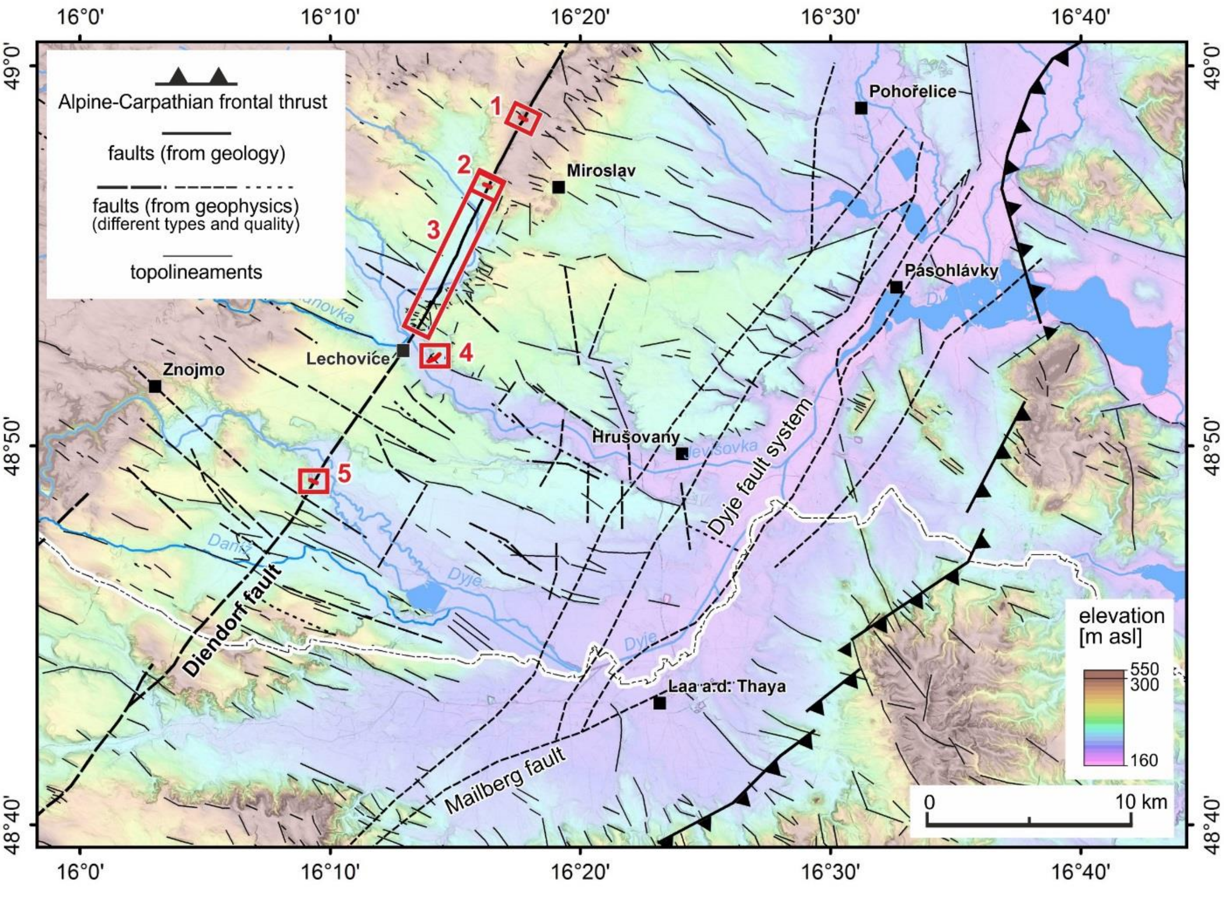

***Figure 15**: Map of selected faults, geophysical indications of possible faults and topography with selected topolineaments in the wider Laa-Pasohlávky area. Largely simplified. Red boxes with numbers indicate localities and areas of detailed research mentioned in the following text: 1 – Kadov trench, 2 – Hostěradice trench, 3 – newly mapped section of Diendorf fault, 4 – Lechovice road cut, 5 – Tasovice trench.*

Diendorf fault

Special attention has been paid to Diendorf fault which is the most prominent fault in the wider area of interest with similar strike as the Mailberg fault system (Fig. 15). Being locally well exposed and therefore accessible for direct field research, it can serve as a reference for indirectly assessing the potential activity of other faults in the area for which detailed information is more difficult to obtain.

The Diendorf fault forms the southern part of a 200 km long fault structure, the Diendorf-Boskovice fault system (DBF). The large length, orientation and position close to the long-term mobile Alpine-Carpathian orogenic zone make the DBF a structure theoretically optimal for relaxing stresses generated in the orogenic foreland during the Cenozoic and also theoretically capable of generating large magnitude earthquakes.

Locally developed fault scarps and locally observed depositional patterns and deformation of the Lower Miocene sediments clearly prove that at least the southern section of the DBF was significantly active during the Neogene. The straight-line nature of the fault, relatively strong local manifestations in relief, increased seismic activity in the broader zone between Melk and Krems, and some other observations interpreted as manifestations of active geodynamic processes have led some geologists to conclude that the Diendorf fault is active (e.g., Decker, 1999). In the Czech part of the DBZ, similar conclusions have been drawn mainly on the basis of geodetic measurements (e.g. Roštínský et al., 2013, 2020). In my opinion, however, none of the indications can be considered sufficient to prove active slip on a Diendorf fault.

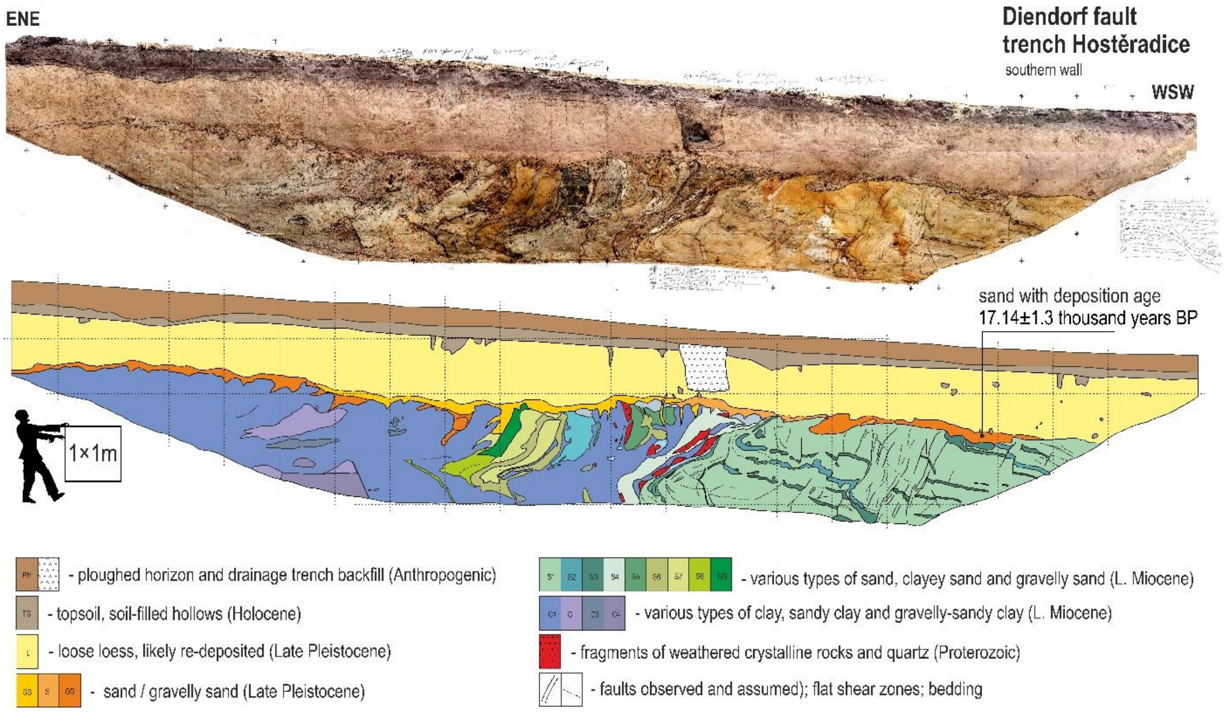

Figure 16. *Geological profile exposed in the Hostěradice trench. Modified from Špaček et al. 2017. Intact sediments overlying the fault provide evidence against local surface faulting during the last 17 000 years.*

Since 2015, we have been conducting systematic research on late activity in the Czech part of the Diendorf fault. Investigations in trenches at several localities (Fig. 15) have ruled out surface disturbance of Quaternary sediments by faulting in the period <17-20 Ma (localities Hostěradice, Fig. 16, and Kadov; Špaček et al. 2017) and ≲60 Ma (locality Tasovice; Prachař in Špaček et al. 2018), respectively. However, the possibility of slip on DBF in earlier phases of the Upper Pleistocene have remained open. Observations in the Kadov trench (Fig. 15) suggest that the fault may still have been active after the deposition of sediments dated at ~100 ka (Špaček et al. 2017). Our new field studies have focused on the area of the Dyje-Svratka basin, where Quaternary sediments are abundant and offer some potential for the study of older Quaternary fault slip. In particular, we have mapped the fault strike in detail by shallow geophysical survey in a flat area without fault scarp between Hostěradice and the Jevišovka valley (Fig. 17). In the northern vicinity of Lechovice, we then focused the research on the detection of faulting of older fluvial accumulations.

Mapping was necessary to clarify the exact course of the fault which was not known and most detailed geological maps do not even show the fault. The fault was indicated in the resistivity and "inphase" maps (the latter parameter is a dimensionless proxy of magnetic susceptibility), which were obtained by EM conductivity measurements at shallow depth in a 150-350 m wide belt. Examples of interpolated resistivity and inphase maps are shown in Fig. 17.

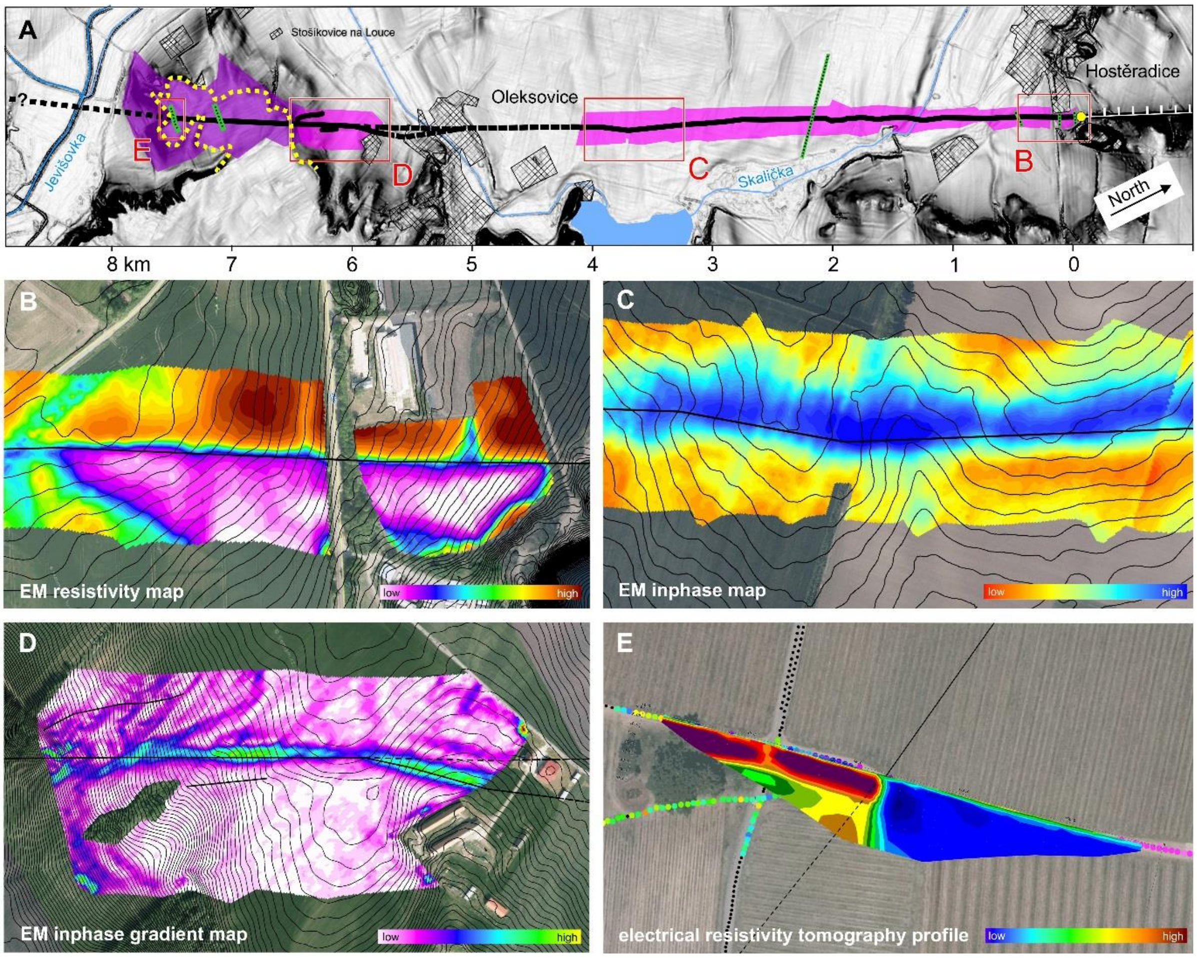

Figure 17. Examples of investigation results of the Diendorf fault in the section north of Lechovice (comp. Fig. 15). The fault trace is shown by black line in all figures. ***A*** *– map of the fault section under study. Areas mapped by different EM conductivity meters highlighted in magenta and violet. ERT profiles shown by green lines. Extent of investigated Middle/Lower Pleistocene sandy gravels shown by yellow dotted line. Red boxes indicate the areas shown in B to E.* ***B, C, D*** *– example results of EM mapping using different data and processing in the areas indicated in A.* ***E*** *– example of ERT profile (vertical profile embedded in the map) showing a steep dip of the fault.*

The newly mapped section of the fault is almost 8 km long. The fault is typically very pronounced as a jump in resistivity and inphase, which is in good agreement with the sharp contact between sands and clays observed in the Hostěradice trench (Fig. 16). Locally, the fault is verified by electrical resistivity tomography (ERT) profiles. The fault course is straight, undisturbed by transverse faults, with few azimuth changes of ≤15°. The dip of the fault implied by the ERT profiles and the trench is about 60° to WNW in the northern part and about 80° or steeper in the southern part (comp. Fig. 17).

North of Lechovice, the fault trace runs through a body of sandy gravels with an uneven base and a flat surface at a relative height of 38-53 m above the floodplain of the Jevišovka river. According to the stratigraphic classification of Zeman (1974), this body largely corresponds to the so-called older sand gravel sheet, whose age is estimated at >900 ka (Early Pleistocene, Donau glacial stage; e.g., Dornič, 1985). The focus of our further research was to determine the interaction of the fault with this stratigraphic marker. We first determined the exact extent of the gravels by geological surface mapping and verified that the surface extent of the gravels is not affected by the fault. We then made detailed ERT measurements on two profiles with 2 m electrode spacing to assess the continuity of the accumulation layer in vertical sections. The thickness of the body is very small and the method used is thus probably at the limit of resolution for the studied structure. The results of the measurements on the two profiles are contradictory, but it can be concluded that if the base of the gravel body is indeed vertically displaced by the fault, then very likely only by less than 2 m. At the same time, such a large displacement seems unlikely given that the gravel surface is now completely flat. Horizontal displacement could not have been assessed at the site.

Despite the persistent lack of clear evidence on the exact age of the latest slip on the fault, the combined geological and geomorphological evidence indicates that the slip rate and seismicity rate of the fault must be very low in the long term, and the observed seismicity rate (see Section 2) can therefore be considered sufficiently representative to assess future seismicity.

3.2 Paleoearthquake record

For intrinsic earthquakes with normal focal depths, surface rupture usually occurs at magnitudes M>6. Therefore, in the seismically weakly active study area, the magnitude interval between the strongest historical earthquakes and the weakest surface-rupturing paleoearthquakes is poorly mapped. In part, this information gap can be supplemented by additional indirect observations of the geological record of strong tremor that may occur at local to regional distances from the epicentre. An important type of structures that are used for this purpose are manifestations of paleo-liquefaction.

Liquefaction is a common phenomenon accompanying stronger earthquakes, affecting some types of water-saturated unconsolidated sediments, especially sands with uniform grain size. Liquefaction, i.e. temporary loss of shear strength, occurs in these sediments due to an increase in pore water pressure and disruption of the grain support structure during periodic internal deformation of the rock by passing elastic waves. Macroscopic deformation of fluidized sediment horizons (and overlying strata) leads to the formation of characteristic structures within and on the surface of sedimentary bodies (e.g. Obermeier 2001).

As of this date, I am aware of two cases of observations of structures in Quaternary sediments in the Czech Republic, interpreted as liquefaction due to strong earthquake tremors. Both observations were made at sites in close proximity to the Diendorf fault. The first is a thin clastic dyke cutting through the lower part of sedimentary sequence of unclear age (Quaternary and Tertiary?), found by I. Prachař in a deep trench crossing the Diendorf fault near Tasovice (Fig. 15) and described and interpreted in an unpublished report of Špaček et al. (2018). The second, more significant record observed at Lechovice, at a distance of <1.5 km from the Diendorf fault, is described below.

Liquefaction and lateral spreading in Lechovice

The findings were made in a road cut on the outskirts of the village of Lechovice (Fig. 15), where faulted Miocene and Quaternary sediments and associated liquefaction structures were documented during the construction of a bypass road. The section exposed a profile 3-5 m high and about 200 m long in the northeastern slope of the Jevišovka valley. A more detailed study of a 25 m long section near the southern end of the profile exposed a sequence of subhorizontally deposited sands to silty sands of Lower Miocene age overlain by thin beds of gravelly sands and loamy sands of apparent Quaternary age (Fig. 18a).

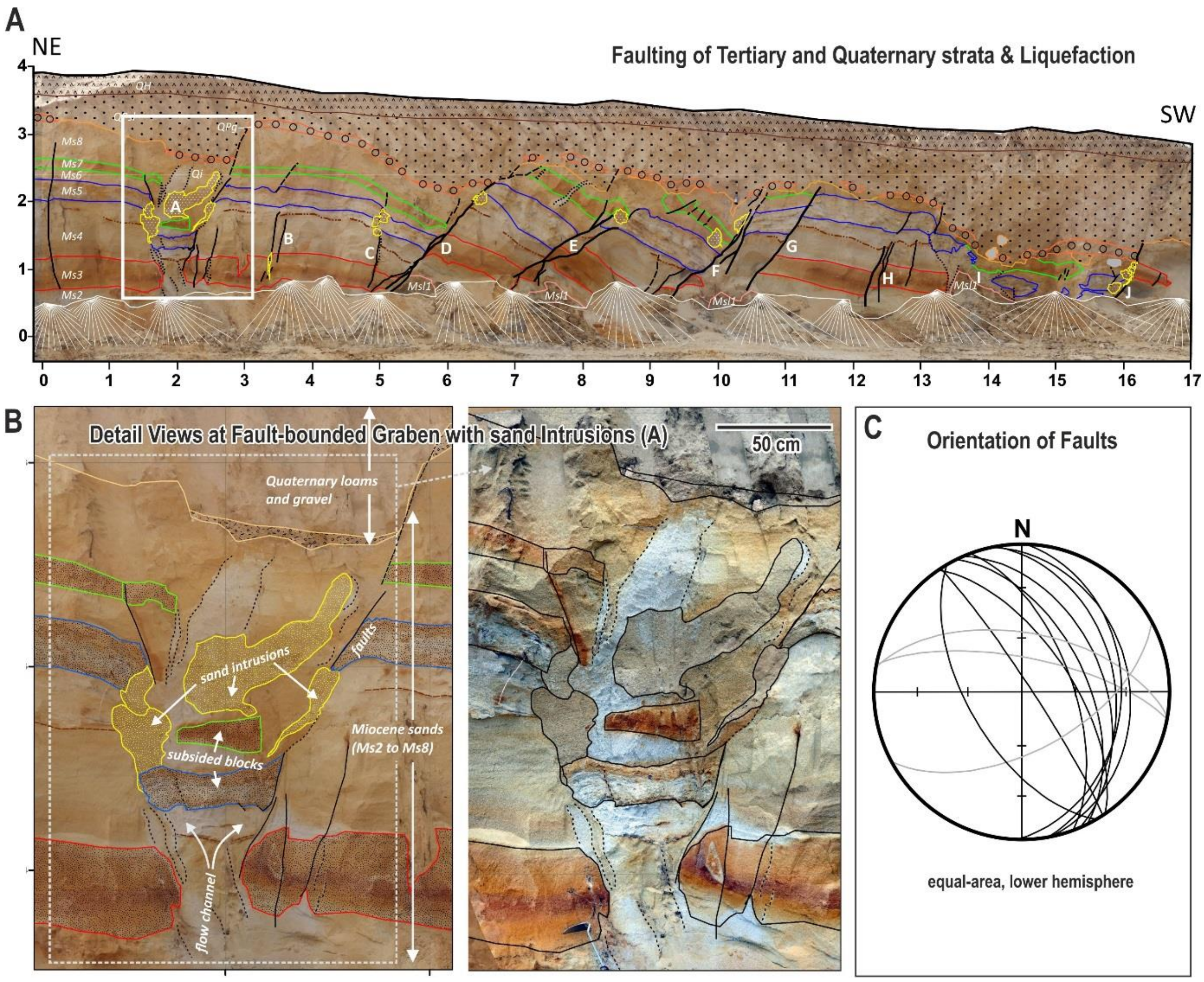

Figure 18. *Observation of faults and liquefaction manifestations in the road cut east of Lechovice (location of the profile schematically marked by the red line in Fig. 15).* ***A –*** *Photomosaic of the exposed profile in the south part of the road cut with important stratigraphic horizons marked by coloured lines and indices. Pockets of sand interpreted as intrusions are highlighted with yellow lines. Faults and steep lithological interfaces are shown by black lines.* ***B –*** *Detail of graben structure with sand intrusions (area indicated by a box in A). On the right with high resolution and true colours, on the left with main features explained.* ***C*** *– Stereographic diagram showing the orientation of faults in the above shown part of the profile (black arcs).*

The Miocene strata and the lower horizons of Quaternary sediments are faulted by a system of NE-dipping faults (typical azimuth 155-175°, Fig. 18c) into several blocks that are rotated up to 35° from the horizontal. In the proximity of many of these faults sharply separated, elongate to isometric pockets of fine-grained sands occur systematically, which are apparently intrusions of fluidized sands derived from deeper levels of the Miocene sequence. Some of these intrusions occur directly within the fault surface and closely follow their local orientation. An important structure is the system of steep divergent faults bounding the subsidence trench in the northeastern part of the profile (Figure 18a - Structure "A" and Figure 18b). Within this graben, there are several pockets of sand intrusions of considerable volume in the upper part.

The collocation of these sand intrusions with faults, and especially with the trench structure, indicates a contemporaneous, causally linked origin. The only satisfactory explanation for the formation of these structures appears to be liquefaction due to strong shaking and simultaneous shear on the faults related to rotation of the rock blocks. The observed structures suggest a likely origin due to lateral spreading which is characteristic of coseismic deformation of water-saturated sandy alluvial sediments in the vicinity of the river channel (the 2010-2011 earthquake sequence around Christchurch is a typical example, e.g. Quigley et al. 2016).

Dating of the Quaternary layers in the studied profile is problematic because the observed gravel relics are not related to any distinctive morphostratigraphic features and they are not necessarily located in the place of original deposition. Assuming the in situ position of the gravels, their age can be considered to be approximately Mindelian (Elster Glacial, MIS10-12; ca. 340-480 Ma). Otherwise, the minimum age of final deposition may be estimated at ca. 15 ka (latest intense solifluction). A higher age seems more likely for the origin of lateral spreading, as the sediments of the studied profile were close to the Jevišovka river channel and were thus largely saturated by groundwater.

Inferred intensities and magnitudes

In the case of abundant observations, a quantitative estimate of the intensity of the shocks can be made based on empirical scaling models taking into account the nature, relative abundance and geographical extent of the observed liquefaction structures. The data obtained allow only a very rough estimation of the minimum intensity. Small structures such as the subsurface clastic veins observed at Tasovice have not been intensively studied worldwide and quantitative calibrations for them do not exist. For this locality, I consider the conservative value of Imin=5-6° as the minimum intensity value of tremors with observed surface manifestations of liquefaction given in Galli (2000).

For the Lechovice site, assuming lateral spreading mechanism, I estimate the minimum intensity for the site to be PGA=20%g (duration of the shaking is not considered) based on the observed correlations in the well-studied Christchurch 2010-2012 earthquakes (Quigley et al. 2016). This value is comparable to the typical value I=7° for the intensity of shaking at sites of lateral spreading reported in Keefer (1984).

Observations of remote manifestations of paleoearthquakes in the region of interest are still rare. It is therefore not possible to assess the geometry of the affected area and thus to directly determine the source of the seismic events. Hypothetical tremors could have been caused by the effect of a local earthquake or as a result of the passage of seismic waves from stronger earthquakes with epicentres at greater distances. In our region, the Eastern Alps or the Vienna Basin (comp. Hintersberger et al., 2018), for example, could be considered as a source of such earthquake. If a local source on the Diendorf fault is assumed, magnitudes of M>4 and M>5.5, respectively, can be considered based on the minimum intensities estimated above.

4 Seismotectonic model

Petr Špaček

The seismotectonic model is used to estimate future natural seismicity in the area of interest. The model takes into account all direct and indirect observations of natural seismicity – historical and instrumental seismicity and interpreted paleoseismicity – in a tectonic context. From these data a model of the main seismogenic sources of the wider area of interest is created and parameters for the inner Laa-Pasohlávky area are derived. In this report, the model of areal sources is briefly described. Models of individual fault seismogenic sources with larger maximum magnitude values is being prepared in parallel and not included here.

For the modelling of areal seismogenic sources, a classical procedure was used:

1) Defining areal zones with a more or less internally homogeneous level of observed seismicity (completeness of the catalogue and density of earthquakes in time and space) and an assumed internally homogeneous seismotectonic style, and,

2) Subsequent parameterization of the seismicity of these zones according to the Gutenberg-Richter (GR) model of magnitude-frequency distribution.

We adopt zones with geometry as defined for SHA Czech Republic (Špaček and Vackář in prep.). These are shown in Fig. 19.

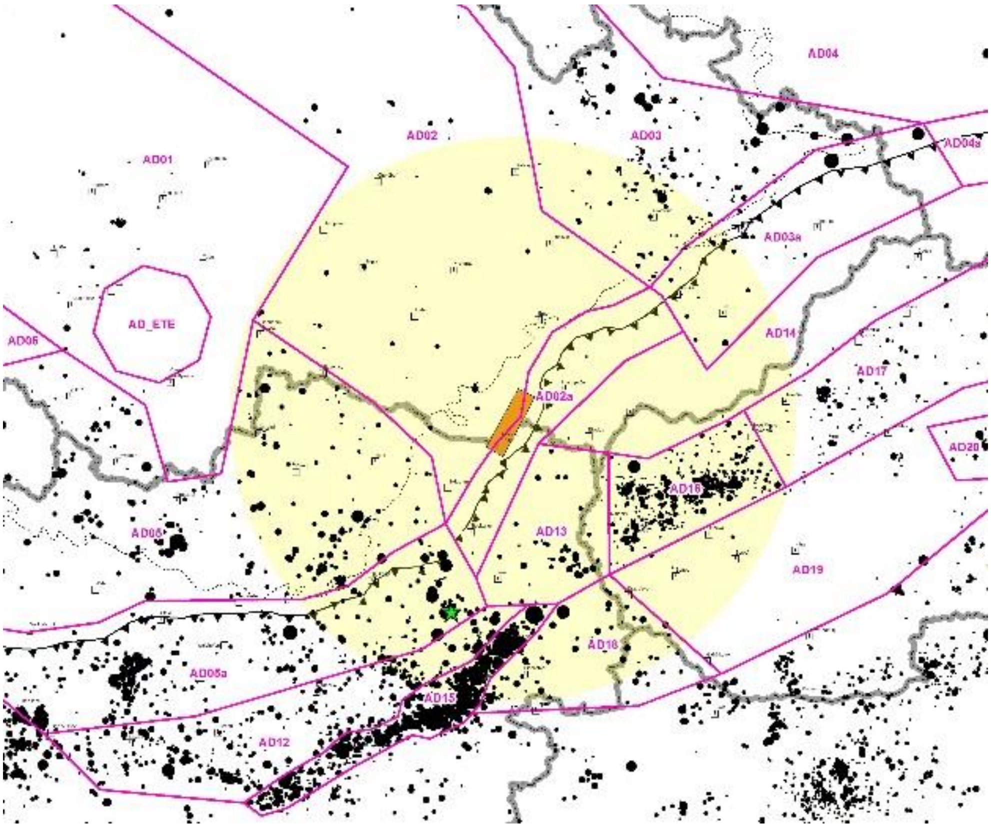

Figure 19. *Map of areal seismogenic sources. Modified from Špaček and Vackář in prep. Magenta polygons - zones of areal seismogenic sources; black dots - earthquakes from local catalogues and regional catalogue compiled by J. Pazdírková; orange rectangle - inner area of interest Laa-Pasohlávky (30×8 km area); yellow circle - broader region of interest within 150 km from the inner area.*

Parameters of more distant zones were also adopted from Špaček and Vackář in prep., those of the near zones being updated using new catalogues, compiled in this project. Seismicity rate in each zone is assessed based on a catalogue of instrumentally recorded earthquakes.

The subcatalogue of earthquakes of a given zone is first classified into several equally sized magnitude classes (0.4 magnitude units). Based on the time evolution of the seismicity rate, the epoch at which the catalogue is complete for a given magnitude range is estimated for each magnitude class. Within the epochs so determined with a complete catalogue record, the mean annual number of events in that magnitude class are then determined, from which a cumulative magnitude-frequency distribution model is constructed, unbiased by the effect of catalogue incompleteness. In low seismicity zones, we attempt to adopt completeness models from more active regions and take a conservative approach to its modification to stabilize the variability of the completeness model across the zones.

In this (sparsely sampled) distribution, the GR equation $\log N = a - b * M$ was fit by linear regression, where M is the local magnitude, N is the number of events with magnitude ≥M, and *a* and *b* are the parameters of interest. In the case of a small number of events in the zone, the parameter *b* is set to a regional mean with a relatively wide a priori tolerance of 0.1 or 0.15 (the value is chosen based on the number of events and the linearity of their distribution). In the zones close to Laa-Pasohlávky, *b* is set to 1, partly based on observations and partly on the assumption of similarity to the seismicity of the Bohemian Massif. The uncertainty of parameter *a* as a function of the tolerance of parameter *b*, the size of the earthquake sample N and the uncertainty of magnitude determination M±0.3, is estimated by stochastic simulation.

Selected parameters of zones within 50 km are given in Table 3.

Table 3. *Selected parameters of seismogenic source zones within 50 km from Laa-Pasohlávky area (see Fig 19; largely adopted from Špaček and Vackář, in prep.)*

Zone	*b*	*a*	a_{norm}	M_{obs}	M_{paleo} or I_{paleo}
AD02	1.00±0.15	1.20±0.10	-0.16	M_L2.5; M_I3.4	I≥7[2]
AD02a[1]	1.00±0.15[1]	0.33±0.10[1]	-0.16[1]	M_L0.9	
AD05	1.00±0.10	2.45±0.13	1.13	M_I4.1; M_L3.6	
AD05a	1.00±0.10	2.60±0.08	1.62	M_I6.0 or 6.06; M_w3.7; M_L4.2	
AD13	1.00±0.15	1.80±0.12	1.33	M_L3.0; M_I3.0	M_w≈6.8±0.5[3]
AD14	1.00±0.15	0.65±0.14	-0.29	M_I5.44; M_L1.3	
AD16	1.00±0.10	2.20±0.03	1.75	M_I5.7; M_L3.4	

b – b-value of GR relation; mean±tolerance

a – a-value of GR relation; mean±standard deviation;

Note: Parameters *a* and *b* are related to local magnitude M_L.

a_{norm} – parameter *a* normalized to area; $a_{norm} = a - \log(\text{area}[\text{km}^2]/1000)$;

M_{obs} – Maximum magnitudes of observed earthquakes adopted from earthquake catalogues. (M_L … local magnitude, M_w … moment magnitude, M_I … magnitude derived from macroseismic intensity).

M_{paleo} or I_{paleo} – Maximum magnitudes or intensities of paleoearthquakes inferred from geological record

[1)] Zone AD02a was singled out in the model of Špaček and Vackář for a purpose not applied here, but was retained for clarity. Value of *b* is adopted from zone AD02 and value *a* inferred from a_{norm} of zone AD02.

[2)] This work and Špaček et al. 2018; [3)] Adopted from Hintersberger et al. 2018.

To model earthquake recurrence over the entire magnitude range, an equation with Mmax can be used, e.g., $N = 10^{a-bM} - 10^{a-bMmax}$, where Mmax is maximum magnitude, here set to a very pessimistic range of 5.5±0.5.

The earthquake recurrence model for the inner Laa-Pasohlávky area is shown in Figure 20. The model shows a very low annual frequency – for example, an earthquake with M=1 should not recur significantly more often than once every 90 years. The values should be taken as an approximation for long-term observations - in the short term, natural variations of seismicity rate become more apparent.

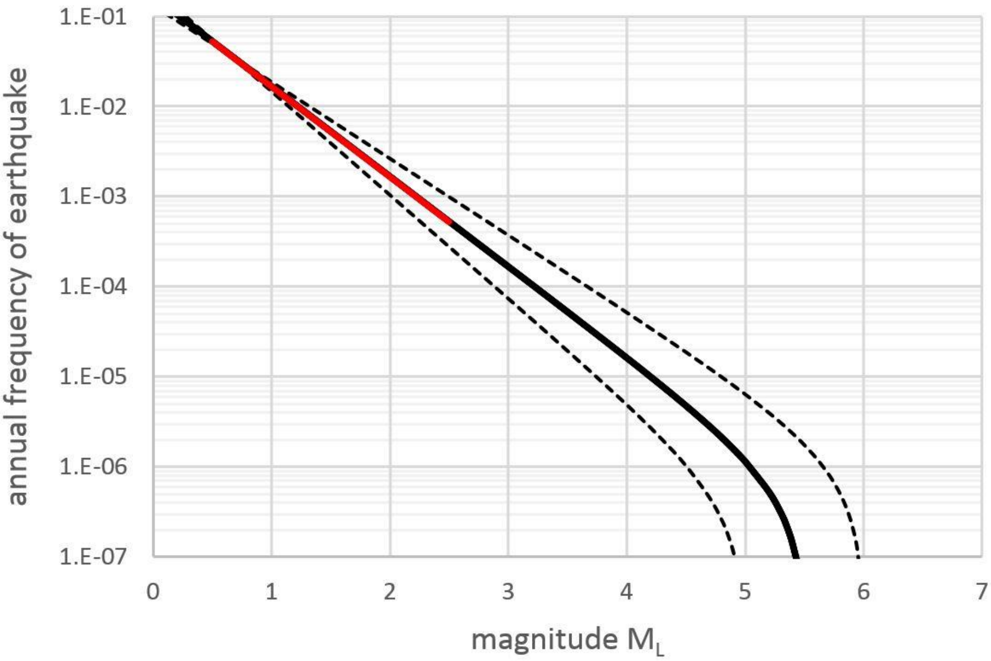

Figure 20. *Natural earthquake recurrence model (mean±1σ) for the inner Laa-Pasohlávky area (30×8 km; as defined in Fig. 19). Based on parameters* a_{norm}*=-0.16, b=1.00±0.15 and Mmax 6.0±0.4. Red line shows the section of the model directly constrained by local catalogue.*

5 Attenuation of seismic waves

5.1 Isotropic Intensity Attenuation Model for the HTPO Region

María del Puy Papí Isaba

In this section we present an Intensity Attenuation Model (IAM) derived for the HTPO study region.

For that, we collected all Macro/Intensity Data Points in the study region to create a macroseismic catalogue for the HTPO-region to later on calibrate an intensity decay law with the distance from the source.

5.1.1 Data: Macro/Intensity Data Points (M/IDPs)

We collected the Macro/Intensity Data Points (M/IDPs) from the Austrian (AEC) and Czech (IPEC) earthquake catalogues (see Section 2.1).

We collected a total of 546 felt earthquakes between 1000 to 2017. From these earthquakes, 108 occurred between the years 2000 to 2017 (107 were extracted from the AEC and one from the IPEC). Before 2000, we gathered 408 earthquakes; 216 were obtained from the IPEC and 192 from the AEC.

For calibrating the IAM, we selected events after 1900 which fulfilled the following criteria:

<u>Intensities greater than and equal to III were used.</u> Although, a large scatter is encountered for low-intensity values, the I0 = III intensity threshold was selected due to the small number of strong earthquakes and, therefore, few numbers of IDPs with epicentral intensities larger than IV. Having chosen an intensity threshold of IV (Pasolini et al. 2008) or higher would have led to a minimal dataset.

<u>Events with more than two IDPs were kept</u> but they were exclusively used for the epicentral intensity calibration and not for the decay-law adjustment. For the intensity decay law calibration, events with more than 10 IDPs were used.

To ensure the exclusion of seismic events associated with mining, quarry blasts, rockfalls, etc. Only <u>earthquakes with depths greater than 1 km were included</u> in the computations (events with no depth information were removed).

<u>Events with epicentres located inside the study area were kept</u>.

In summary, the dataset contains 41 earthquakes (Fig. 21) with local magnitudes between 1.8 and 5.4 and over 2,500 IDPs, whose intensity values vary between III and VII-VIII (EMS-98, Fig. 22). In addition, the dataset includes other focal parameters (location and time of the earthquake) and the location of the IDPs.

Table 4 lists the earthquakes which were used to calibrate the IAM.

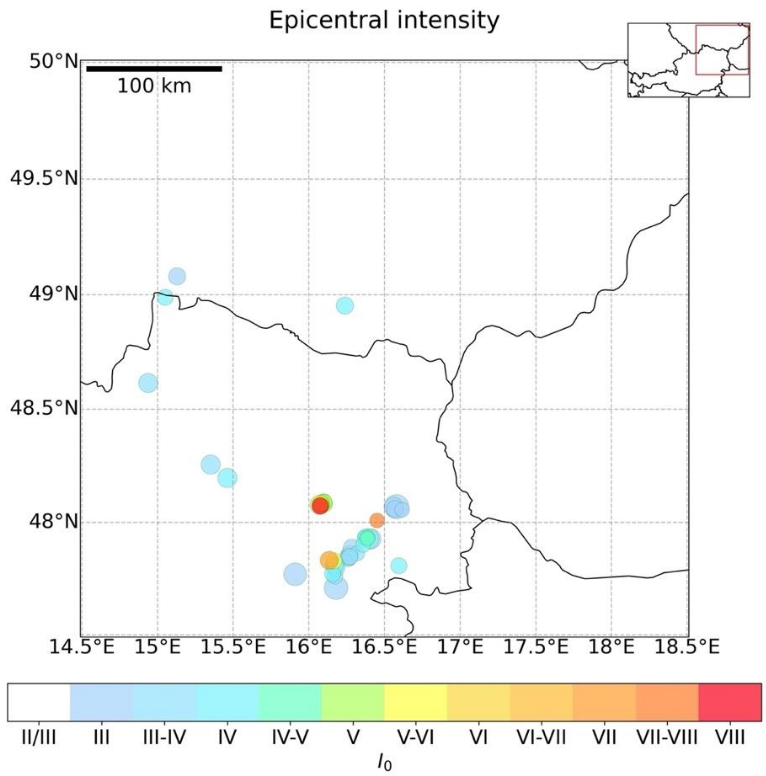

Figure 21. *Epicentres of earthquakes from 1925 to 2017. These earthquakes will be used in the IAM calibration. Local magnitude ranges between 1.8 and 5.4 and depths between 2 and 15 km.*

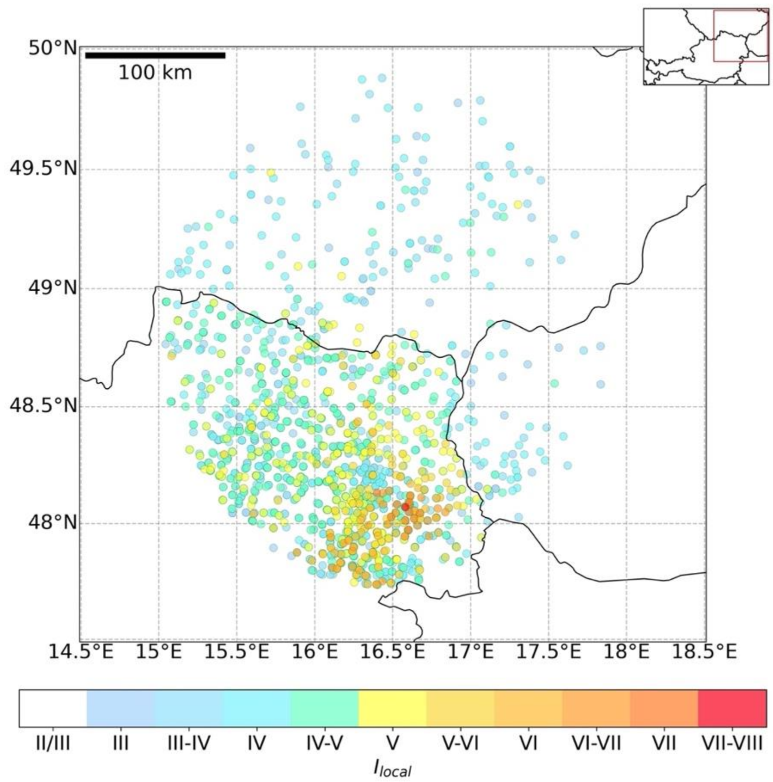

Figure 22. *Intensity Data Points (IDPs) of earthquakes whose epicentres are shown in Fig. 1. The intensity scale is the EMS-98.*

Table 4. *Earthquakes and their characteristics used to calibrate the IAM for HTPO.*

Number	Year	Month	Day	Hour	Min	oriLat	oriLon	M_L	I0	depth
1	1925	1	20	18.0	40	49.08	15.13	2.6	3.0	2.0
2	1927	10	8	19.0	49	48.07	16.58	5.4	8.0	9.0
3	1939	9	18	0.0	14	47.77	15.91	4.8	7.0	10.0
4	1972	4	16	10.0	10	47.71	16.18	5.1	7.5	9.0
5	2001	6	7	3.0	27	47.86	16.27	2.8	4.0	8.0
6	2001	11	21	17.0	10	48.07	16.56	3.5	5.0	8.0
7	2004	4	26	20.0	58	48.06	16.57	2.6	4.0	9.0
8	2006	6	30	17.0	55	47.842	16.256	2.4	4.0	15.0
9	2007	9	28	0.0	37	47.848	16.267	2.6	4.0	10.0
10	2008	10	14	5.0	21	47.888	16.285	2.6	4.0	8.0
11	2009	1	18	16.0	53	48.057	16.616	2.4	3.0	4.0
12	2009	10	20	0.0	14	47.863	16.32	1.8	3.0	7.0
13	2009	11	19	8.0	0	47.848	16.272	2.5	3.5	13.0
14	2010	9	5	10.0	24	48.615	14.939	2.9	5.0	5.0
15	2010	10	11	19.0	8	48.256	15.352	2.3	5.0	5.0
16	2011	2	22	0.0	31	47.762	16.172	2.3	3.5	14.0
17	2013	9	20	2.0	6	47.927	16.41	4.3	5.5	11.0
18	2013	10	2	17.0	17	47.928	16.397	4.2	5.5	12.0
19	2013	12	11	17.0	14	47.799	16.178	3.0	4.5	14.0
20	2014	3	17	20.0	33	48.197	15.462	3.2	5.0	5.0
21	2014	6	1	0.0	43	48.953	16.239	2.0	4.0	3.0
22	2014	6	8	21.0	57	47.81	16.17	2.7	4.5	8.0
23	2014	12	27	9.0	38	47.808	16.595	2.0	3.5	8.0
24	2015	3	19	19.0	21	48.989	15.051	1.7	3.5	5.0
25	2015	8	15	15.0	33	47.933	16.369	2.3	3.0	14.0
26	2015	8	15	15.0	35	47.938	16.375	2.4	3.0	14.0
27	2015	10	26	11.0	49	47.772	16.158	2.4	3.5	9.0
28	2016	1	16	16.0	16	47.901	16.359	1.6	3.0	12.0
29	2016	2	24	13.0	45	47.934	16.389	2.0	3.0	11.0
30	2016	2	24	16.0	17	47.929	16.386	2.0	3.0	8.0
31	2016	4	25	5.0	40	48.095	16.097	1.8	3.0	10.0
32	2016	4	25	10.0	28	48.078	16.071	4.2	5.0	10.0
33	2016	4	25	10.0	49	48.086	16.098	2.5	4.0	8.0
34	2016	4	26	3.0	40	48.082	16.103	2.2	3.5	11.0
35	2016	4	27	7.0	48	48.091	16.104	2.0	3.0	12.0
36	2016	5	10	5.0	41	48.082	16.089	2.3	3.0	8.0
37	2016	5	10	5.0	52	48.0840	16.078	2.7	3.5	10.0
38	2017	7	29	21.0	40	47.83	16.166	1.8	3.5	6.0
39	2017	7	29	23.0	22	47.832	16.135	2.4	4.5	5.0
40	2017	10	23	23.0	35	48.009	16.451	2.3	3.0	11.0
41	2017	11	8	18.0	36	48.074	16.076	3.1	4.0	9.0

5.1.2 Method

Local magnitude homogenization

To define a homogeneous magnitude type (ML) for the calibration of hte Inetensity Attenuation Model, we considered the linear regression relations between institute pairs presented in section 4 where different magnitude values for the same earthquakes located by four different organizations (ZAMG, IPE, SEK and SAV) in the study region were compared.

Epicentral intensity calibration

The first step to compute the IPE was to calibrate the epicentral intensity according to the local magnitude (M_L) and the focal depth (z) (Eq. 9). The main reason is that the epicentral intensity does not always equal the maximum reported intensity (I_{max}),

$$I_{max} = k_0 + k_1 \cdot M_L + k_2 \cdot ln(z[km]) \pm \sigma_0 \qquad [9]$$

Where k_0, k_1 and k_2 are empirical constant derived from eq.1 calibration. $\sigma$is the standard deviation of the IPE.

The linear-logarithmic regression was calculated using an Ordinary Least Square Adjustment (OLSA) following the interpretation of Shebalin (1958) and using earthquake epicentres located in Austria (Tab. 4), as input parameters.

Attenuation of local intensity: decay law

The intensity distribution on the earth's surface depends also on the ground attenuation with increasing distance. The origin of the attenuation model for point sources dates back to Kövesligethy (1907) and Sponheuer (1960) and was used in Europe by Arroucau et al. (2006) for Metropolitan France, Pasolini et al. (2008) in Italy and Stromeyer and Grünthal (2009) for Central Europe, among others.

In this step, the difference between the modelled epicentral intensity (I_0^{IPE}) and the reported local intensity (I_{local}) was adjusted to the following expression (eq. 10):

$$I_{local} - I_0^{IPE} = c_1 \cdot ln(R/z) \pm \sigma_{local} \qquad [10]$$

Where c_1 is an empirical constant determined by weighted OLSA and R is the hypocentral distance from the source to the IDP location, which must be given in same units as the focal depth (z) in equation 10.

By giving more weight to the data close to the epicentre, which usually has higher local intensity degrees, we secure a better mapping of the epicentral region, i.e. usually larger intensity values. This approach was applied to compensate for the large number of IDPs with low-intensity values when moving away from the epicentre and the high-intensity values and little available data around the epicentral region. The weight matrix used in this OLSA was defined by setting weights, inversely proportional to the number of IDPs (N) of each earthquake, in the matrix diagonal, following the expression (1/N). However, it must be noted that, when following this approach, the error of the intensity estimation in regions far away from the epicentre is also increased. The weight matrix was constructed by dividing the dataset into three different subsets. The first subset encloses local intensity values between III and IV, the second subset all intensities between IV and V, and the third subset all IDPs with local intensities greater than V.

5.1.3 Intensity Attenuation Model

IPE empirical constants and standard deviation resulting from both OLSA are presented in Table 5.

Table 5. *IAM empirical constants, epicentral and local intensity standard deviation and local intensity bias.*

k_0	k_1	k_2	c_1	σ_0	σ_{local}	I_{local} **bias**
1.82	1.24	-0.50	-1.20	±0.5	±0.60	-0.3

Figure 23 shows the epicentral (a) and local (b) intensity residuals for the data set, which follow a normal distribution. For the epicentral intensity, the distribution is centered at zero and has a standard deviation of about 0.5. The residual values vary between -1.1 and +1.2. These significant differences between reported and modelled epicentral intensities might be, among other reasons, because the epicentral intensity is assigned based on the maximum local intensity (maximum reported intensity), which may not coincide with the intensity at the epicentre.

On the other hand, local intensity standard deviation ranges a bit more, approximately from -2 to +2 degrees. A plausible reason could be the potential presence of site-effects induced by local geostructural conditions. Besides, the presence of a bias in the local intensity residuals might be corrected with the computation of a geology correction as in Isaba et al. (2020).

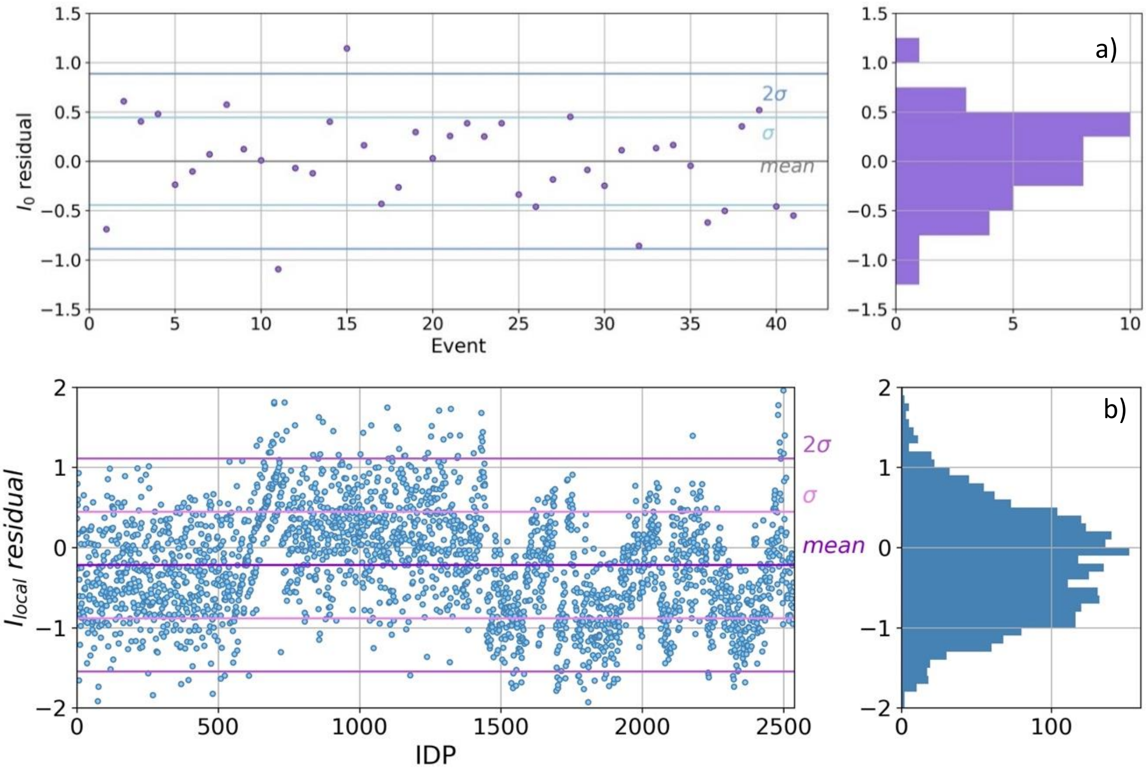

Figure 23. a) *Epicentral intensity residuals. The grey line indicates the bias (nil) of the epicentral intensity. The light blue lines indicate the standard deviation of the epicentral intensity ($\sigma_0 \pm 0.5$). The dark blue lines indicate two times σ_0.* ***b)*** *Local intensity residuals. The purple line indicates the bias (-0.3) of the local intensity. The light pink lines indicate the standard deviation of the local intensity ($\sigma_{local} \pm 0.6$). The dark pink lines indicate two times σ_{local}.*

5.2 Direction-dependent Intensity Attenuation

Petr Špaček

Many earthquakes in the Eastern Alps (sometimes called "transversal" earthquakes) are characterized by strongly elongated isoseismals, documenting significantly more efficient propagation of seismic waves towards the Alpine foreland than into the orogen.

We have analysed a dataset of 10 historical earthquakes with well described asymmetry of intensities (9 events with epicentre in E Alps + 1 from W Carpathians far off the Vienna Basin Anomaly; Table 6). We have first interpolated the available cross-border isoseismal maps or data points into intensity grids. For each of these grids intensity vs. distance profiles were constructed along two characteristic directions – direction of maximum and minimum distance to outer isoseismal in the Alpine foreland (F-direction) and Alpine orogen (O-direction), respectively. In most cases these directions are quasi-perpendicular to the Alpine/Carpathian thrusting front.

Table 6. *Historical earthquakes used for the analysis of intensity attenuation in the two principle directions.*

Earthquake	**Lat**	**Lon**	**I0**	**Intensity data sources**
1858 01 15 Žilina	49.22	18.76	7.5	Procházková and Kárník 1978
1907 03 22 Liezen	47.57	14.46	6	Procházková & Kárník 1978 (Trapp, Lukeschitz)
1916 05 01 Zeltweg	47.18	14.69	7	Procházková & Kárník 1978 (Trapp, Lukeschitz)
1938 11 08 Ebreichsdorf	47.96	16.4	7	Hammerl & Pazdírková, unpublished IDPs
1963 12 02 Ebreichsdorf	47.88	16.37	6.25	Drimmel 1980; Procházková & Kárník 1978
1964 06 30 Semmering	47.65	15.83	5	Drimmel 1980; Procházková & Kárník 1978
1967 01 29 Molln (Kirchdorf ad Krems)	47.88	14.31	6.75	Procházková & Kárník 1978; Drimmel & Trapp 1975
1972 04 16 Seebenstein (Neunkirchen)	47.71	16.18	7.75	Drimmel 1980; Procházková & Kárník 1978
1984 04 15 Maria Schutz	47.64	15.87	6.5	Drimmel 1990
1984 05 24 Gloggnitz	47.65	15.92	6	Drimmel 1990

Fig. 24 shows the results as a distance vs. normalized intensity (I_0-I) plot with median and variation (0.15 and 0.85 fractiles) of I_0-I value distribution along the profiles. We emphasize that we deliberately describe extreme directions in this way while mean values over wider azimuth ranges may differ significantly.

Despite the expected bias in this small data sample combining earthquakes with different focal depths and different quality, the results illustrate nicely and clearly the contrasting seismic wave propagation into the stable European plate with Variscan consolidation and into the Meso-Cenozoic orogen. While at epicentral distances shorter than ~50 km the medians are similar for both F and O directions, at larger distances the curves for the F-direction departs and exhibits a flat part at least up to 250 km. Similar shape with low intensity attenuation at >50 km distance seems to be characteristic for central and eastern North America (e.g. Atkinson and Wald 2007, Atkinson et al. 2014; Fig. 24). There, this feature has been attributed to strong postcritical Moho or intra-crustal reflections whose energy adds to that of Lg waves at certain distance range (see also Burger et al. 1987). Similar mechanism was suggested by Drimmel 1990 for northward propagation of the eastern Alpine „transversal" earthquakes.

Other reference intensity attenuation curves shown in Fig. 24 include the results reported in previous section for the HTPO project region and those of Bakun and Scotti 2006 to illustrate the situation in French analogues of Alps and Variscan Foreland. The results for HTPO region (at z=8km) are similar to older results of Procházková (1982) from our region of interest (not shown in the plot). These curves fit approximately the lower bounds of the intensity range for the earthquakes analysed despite partly overlapping input datasets. This most likely reflects the different approaches to directional dependence analysis (Papi-Isaba did not differentiate by azimuth, Procházková used fixed azimuth ranges while here the F and O directions were used).

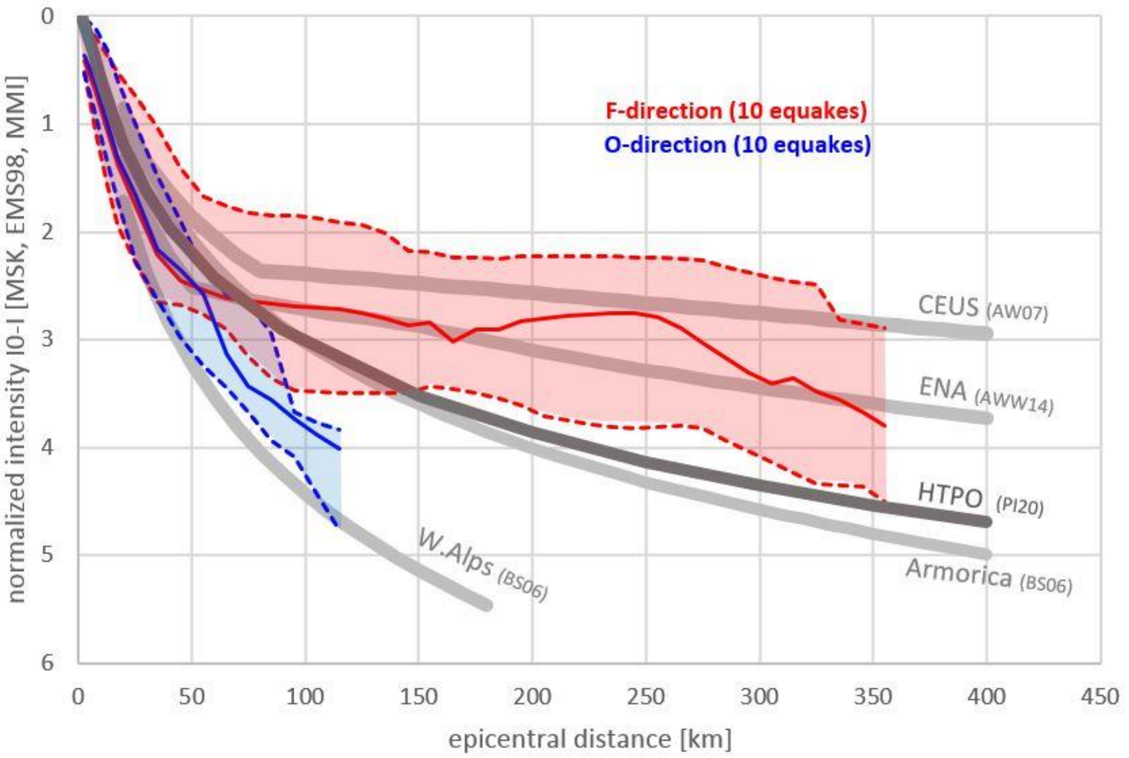

Figure 24. *Intensity attenuation with distance in two principal directions for selected historical earthquakes (modified from Špaček et al. 2021). F-direction and O-direction are directions of maximum and minimum distance to outer isoseist in the Alpine Foreland and the Alpine Orogen, respectively. Data were interpolated from published isoseismal maps as described in text. Intensity values are normalized to epicentral intensity I_0. Thick grey lines show selected published intensity attenuation curves (z=8km) for Central and Eastern US (CEUS), Eastern North America (ENA), Armorica, Western Alps and 150 km perimeter around the Pasohlávky-Laa region (HTPO, see the previous section). AW07 – Atkinson and Wald 2007; AWW14 – Atkinson et al. 2014 BS06 – Bakun and Scotti 2006, PI20 – Papi-Isaba 2020 and this report.*

5.3 Case Study: M_L4.2 2016 Alland Earthquake

Petr Špaček, Pavel Zacherle, Rita Meurers and Jana Pazdírková with support of the AlpArray Group

The asymmetry of seismic energy propagation from the Alpine earthquakes' foci described above poses a complication in modelling the ground motions due to hypothetical future earthquakes. To model the surface effects of future earthquakes, we need to understand this phenomenon and quantify the attenuation as accurately as possible, using instrumental records.

In this effort we analysed the local to regional wavefield of a single earthquake with ML4.2 (ZAMG) / Mw3.7 (Schippkus et al. 2019) and epicentre WSW of Vienna (48.078°N, 16.069°E; near Alland) using instrumental data with unprecedented dense coverage (including the stations of AlpArray project) and rich macroseismic observations. This earthquake exhibits the characteristic asymmetry of isoseismals, its hypocentre is located in the basement of the European plate and epicentre is within ~25 km from that of the regionally strongest historical earthquake, Ried am Riederberg 1590.

Macroseismic data were collected via questionnaires of ZAMG Vienna, IG CAS Prague and ESI SAS Bratislava and processed into intensity data points (IDPs) by R. Meurers and J. Pazdírková (respectively for Austrian and Czech territory). Instrumental records of 215 permanent and temporary stations were used for the analysis and peak ground motions and amplitude spectra within time windows tied to Sg+Lg wavetrains.

Figure 25 shows the interpolated instrumental peak ground acceleration (PGA) and interpolated macroseismic intensity together with position of seismological stations and IDPs.

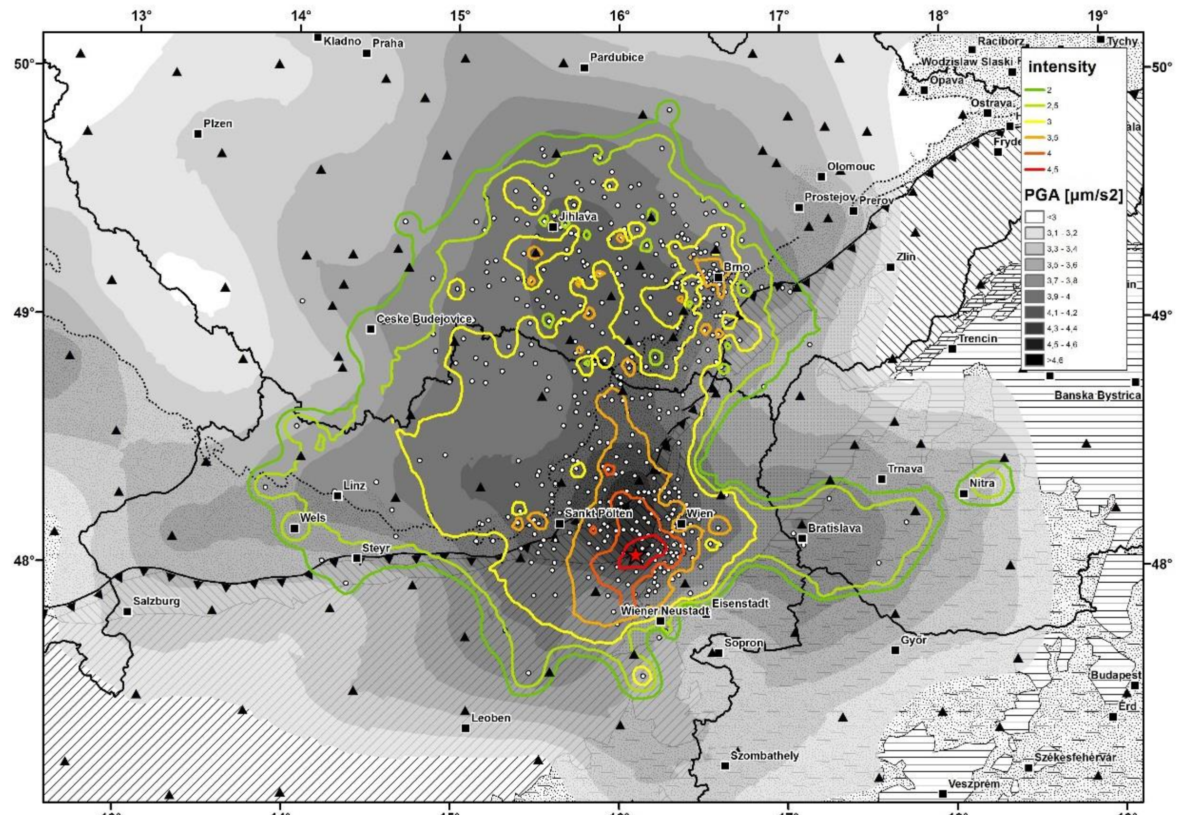

Figure 25. *Map showing the main observations used for the Alland case study. Black triangles – seismic stations. Open circles – IDPs. Interpolated logPGA is shown by shades of grey. Interpolated intensity is shown as contour lines.*

5.3.1 Correlation between Instrumental Ground Motion and Intensity

As seen from Fig. 25, the smoothed high precision instrumental and high spatial resolution macroseismic data exhibit a very good match. To allow joint interpretation of macroseismic and instrumental observations using locally verified relation, we first studied correlation of the instrumental ground motion with intensity. Correlation was performed along defined profiles in regions rich in primary data to easier identify the anomalies. We have correlated the interpolated *PGA* and I_{EMS98} values on 6 radial profiles from the epicentre (azimuth range 280-15°, i.e. mostly in the foreland domain) within the intensity range $2.5 \le I \le 4.3$. A linear regression was calculated for each profile (in agreement with other works, we assume a linear relationship between PGA and I in the range $2 < I_{EMS98} \le 5$). The scatter of the resulting regression lines is rather large (Fig. 26) and the average correlation calculated as a mean of all regression lines excluding one outlier is given by equation 11.

$$\log PGA\ [\mathrm{cm/s^2}] = 0.48 * I_{EMS98} - 1.2 \qquad [11]$$

In Figure 26, our result can be compared with results from other areas. Our relation is reasonably close to some results from other regions, e.g. equations of Faenza and Michelini 2010 or Zanini et al 2019. It must be assumed that the relationship, in addition to the method of data processing and other factors, is also dependent on the frequency content of the ground motion. We expect that the locally derived relationship (eq. 6.2a) may perform better with high frequencies (>10 Hz) predominating in our small magnitude earthquakes.

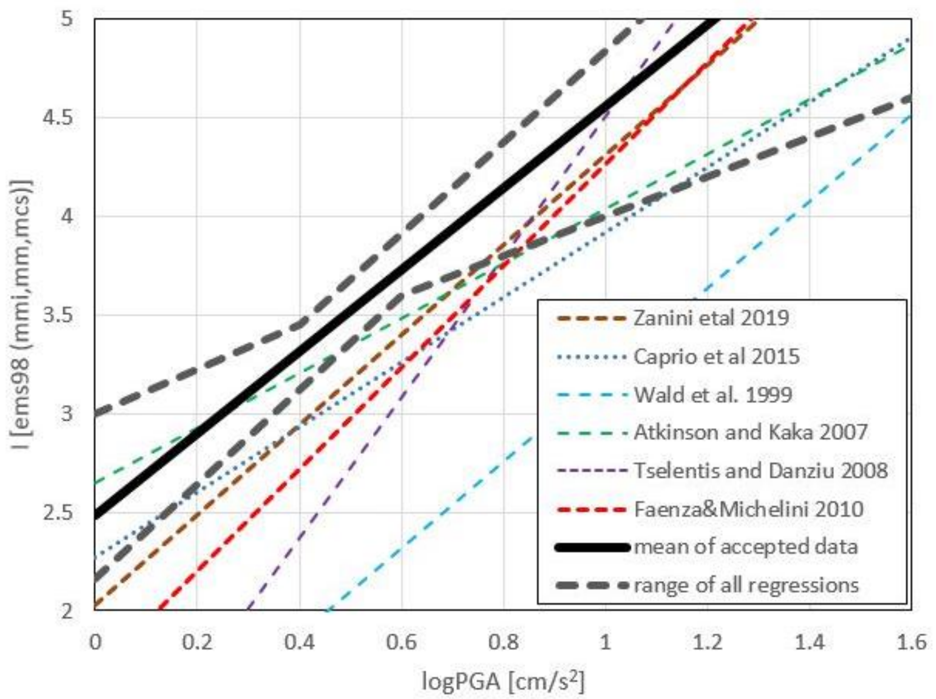

Figure 26. *Correlation of instrumental peak ground acceleration (PGA) and macroseismic intensity. Thick dark lines show results of this study: solid black line – regression of all data (eq. 6.2a); dark grey dashed lines – full range of linear regressions along the profiles. Coloured lines show selected published correlation lines for reference.*

5.3.2 Ground Motion Attenuation Model

As can be seen from Figure 25, we observe a very small decrease of intensity and PGA values at epicentral distance range between 30-50 km and 130-180 km in the direction into the Alpine foreland. On the other hand, a sudden drop of respective values is observed at a distance of 20-30 km in direction to the orogen. The amplitude decrease is accompanied by significant change of spectral content – while high frequency signal at 10-20 Hz is characteristic for the Foreland domain, it is strongly reduced in the Alpine domains.

The effects of site response or the source directivity have been ruled out as primary factors and the contrasts between the seismic energy attenuation in the domains is believed to be due to the contrasts of their deeper crustal structure. While the Alpine crustal structures near the southern margin of stable European plate act as an efficient high-cut frequency filter, towards the foreland, seismic energy propagates easily over the whole spectrum and is apparently amplified anomalously.

Decay of amplitudes with distance in the Alpine foreland is essential for ground motion modelling in the Laa/Pasohlávky region of interest. The basic components of the model we use here are described, for example, in Boore (2003). The amplitude attenuation model is constructed as a product of two effects: 1) frequency-independent geometrical spreading attenuation G(R) and 2) frequency-dependent anelastic and scattering attenuation A(f, R). Owing to interdependence of both components and the limitations imposed by small number of observations, we have to make some simplifying assumptions when searching for their parameters.

The basic shape of the GS curve was determined based on local observations and examples from better explored areas. From the combined distribution of PGA and intensities with distance, it is clear that the curve is segmented and has a flat ramp at about 50-130 km from the epicentre.

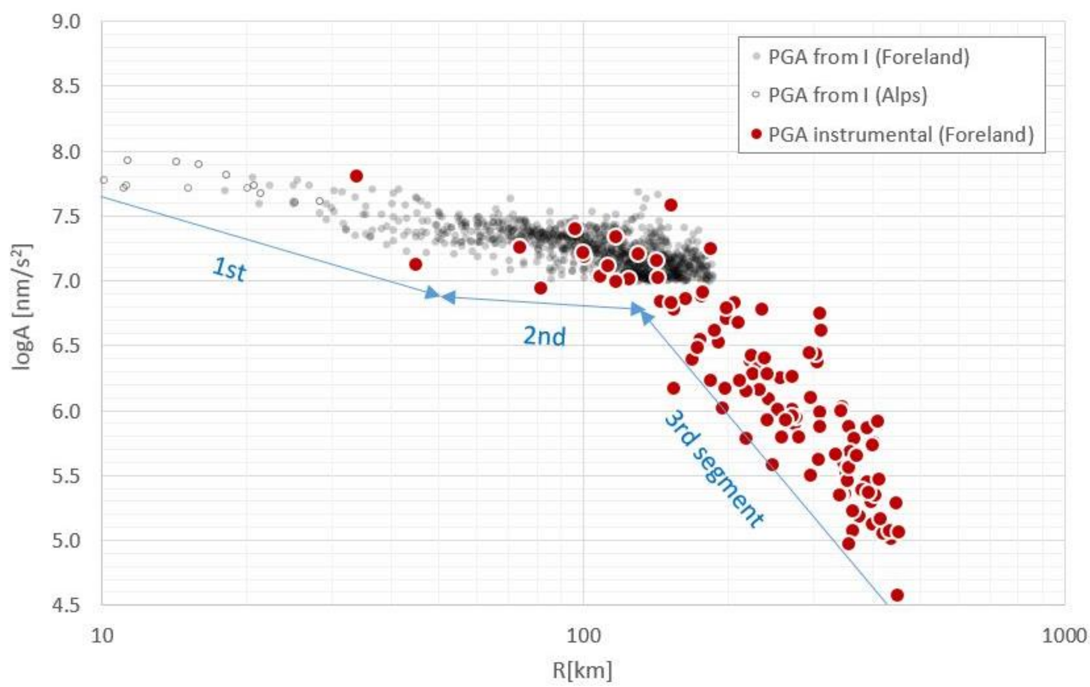

Figure 27. *Log-log plot of the observed instrumental PGA (red circles) and converted macroseismic PGA (grey circles) vs. distance. Macroseismic datapoints are values in the nodes of the interpolated intensity grid converted into PGA using Eq. 11.; only the more reliable values with I ≥ 2.5 are shown. Note the three segments with quasi-linear (i.e. exponential in linear plot) distribution.*

Such flat ramp is in agreement with foreland-direction intensity attenuation of stronger historical earthquakes in this region (see previous section). A similar or more complex segmented geometrical spreading curve with a flat ramp has been modelled in other regions as well (e.g., North America - Atkinson 2004, Switzerland - Edwards et al. 2011, UK - Rietbrock et al. 2013). It can be explained e.g. as an effect of reflection at Moho and intracrustal discontinuities (comp. Burger et al., 1987, for North America or Drimmel, 1990, for the Alpine foreland) or perhaps as a consequence of the superposition of the effect of multiple finite waveguides.

The three-segment GS model for the Alland earthquake is quantified by equations

$$\left.\begin{array}{ll} G(R) = (1/R)^{1.1} & \text{for } R < 50 \text{ km} \\ G(R) = 0.0135 * (50/R)^{-0.7} & \text{for } 50 \leq R \leq 130 \text{ km} \\ G(R) = 0.0272 * (130/R)^{0.5} & \text{for } R > 130 \text{ km} \end{array}\right\} \quad [12]$$

where R is taken here as hypocentral distance in km (taking into account the small size of earthquake source).

The exponent 0.5 in the third segment was set with the assumption of propagation as a surface wave without energy leakage. The exponent 0.7 in the second, central, segment was set as the optimal value that fully compensates for the observed increase of low-frequency amplitude with distance using the quality factor inferred in the third segment (see below). The exponent 1.1 in the first segment was estimated by a fit to the observed intensity decay.

The anelastic and scattering attenuation is given by equation

$$A(f, R) = \exp\left[-(\pi * f * R) / \beta_{path} * Q(f) \right] \qquad [13]$$

where f is frequency in Hz, β_{path} is the regional Sg and Lg wave velocity (mean value of 3.5 km/s inferred from local travel times) and Q(f) is quality factor as a function of frequency.

The apparent quality factor Q(f) was derived empirically from the frequency dependence of RMS amplitude decay with distance in the third segment of geometrical spreading model described above. It is simplified into exponential form,

$$Q = 315 * f^{0.40} \qquad [14]$$

and extrapolated throughout the whole region of interest.

The Fourier amplitude $Y(M_0,f,R)$ is predicted by the equation

$$Y(M_0,f,R) = S(M_0,f) * G(R) * A(f, R) * L(f) \qquad [15]$$

where M_0 is the seismic moment, $S(M_0,f)$ is source spectrum and L(f) is site response.

Source spectrum had been modelled as the Brune (ω^2) spectrum at R = 1 km based on source parameters published in Schippkus et al 2019 (magnitude Mw = 3.7; source radius r = 200 m; shear wave velocity in hypocentre β_{source} = 3.3 km/s^2). For site response model, the amplification is neglected and weak high-frequency attenuation (κ = 0.005) is modelled based on observations (see Boore 2003 for details on modelling of the source and site effects).

The resulting model of the Alland earthquake acceleration amplitude decay with distance in the Alpine foreland is shown in Fig. 28 together with the instrumental and macroseismic PGA to illustrate a satisfactory fit.

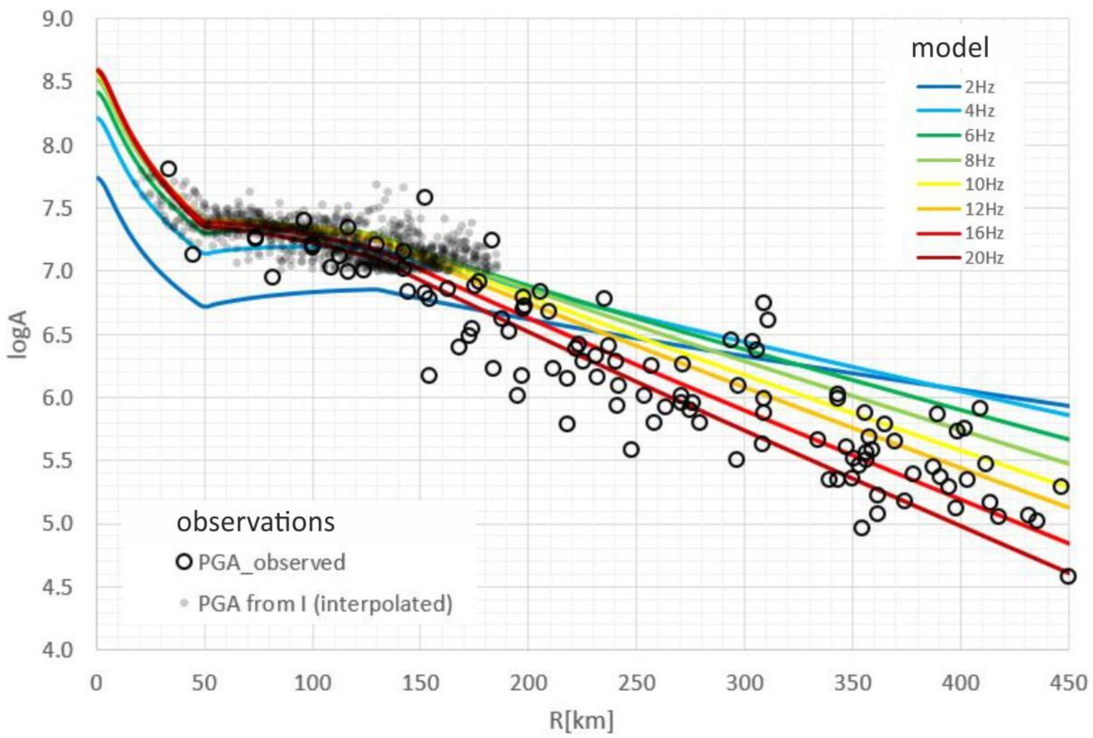

Figure 28. *Observed PGA values (instrumental and macroseismic; see Fig. 27) juxtaposed on the Fourier acceleration amplitude model using Eq. 15 as a function of hypocentral distance R.*

It should be emphasized that due to the lack of earthquakes, we do not yet have observations from small epicentral distances in the foreland domain directly comparable to the Pasohlávky-Laa area. Due to limited number of input data, the model is approximate and its fit to different earthquakes must be further tested and improved.

For the purpose of ground motion modelling, it may therefore be preferable for the time being to rely on adopted models, which are better conditioned by a larger number of observations in the near zone. Therefore, we further compared our results with other models in use from areas with comparable crustal structure. For a distance range of 0-150 km, a satisfactory good agreement of the observed amplitude attenuation with the Fourier amplitude attenuation models for eastern North America (e.g. Atkinson 2004) was found. As their results have been applied in ground motion prediction equations of Atkinson and Boore 2006 or Pezeshk et al. 2011, these latter are expected to perform well in modelling of peak acceleration in the near zone (<150km) of Laa/Pasohlávky area.

6 Induced Seismicity Model

Wolfgang Lenhardt & Fee-Alexandra Rodler

6.1 Mechanics of Induced Seismicity

Geothermal systems are able to trigger seismic events due to changes of pore pressures (e.g. Talwani & Acree, 1985, Davis & Pennington, 1989, McGarr, 1991, McGarr, 1993, McGarr & Simpson, 1997, Lenhardt, 1998, Talebi, 1998, House & Flores, 2002, Trifu, 2002). Several processes can be distinguished:

1) Fluids percolate below water reservoirs and lubricate existing geological faults (reservoir-associated seismicity). This mechanism – involving diffusion – requires an unstable tectonic environment to generate earthquakes.
2) Disposal of fluids or gases via boreholes which requires frequently high pressures in terms of fracking.
3) Extraction of fluids for thermal baths. This case applies to the project HTPO.
4) Usage of juvenile waters from greater depth (> 1000 m, depending on the geothermal gradient) for thermal energy extraction.

Stress regime

Generally, an extraction of fluids leads to a decrease in pore pressure ($\Delta p < 0$, hence stabilizes the stress regime by moving the Mohr circle to the right in Fig. 29), whereas a disposal of water increases the pore pressure ($\Delta p > 0$, hence de-stabilizes the stress regime by moving the dotted Mohr circle to the left [solid circle] towards the instability criterion, indicated by the tilted line in Fig. 29).

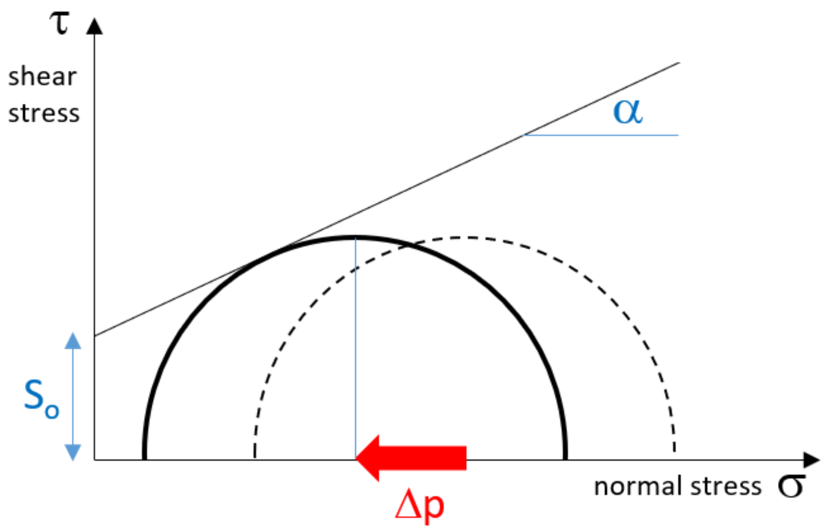

Figure 29. *Mohr's circle and influence of pore-pressure changes (Δp). α denotes the angle of internal friction. So = cohesion.*

Additional important parameters are Poisson's ratio and the uni-axial compressive strength (UCS), which determine the acting minimum and maximum normal stresses (= principal stresses). The dynamic Poisson's ratio ν can be calculated form seismic wave velocities (Jaeger et al., 2007):

$$\nu = (2 - c) / (2 (1 - c)) \qquad [16]$$

with

c… $(vp/vs)^2$, where
vp… P-wave velocity
vs… S-wave velocity

The intrinsic shear strength So Fig. 29 – also called cohesion – together with the angle of internal friction α defines the stability criterion. The latter amounts to approximately 32° (Jaeger et al., 2007) in normal faults below rock stresses of 100 MPa.

The radius of the Mohr's circle is defined by the minimum and maximum principal stress ($\sigma 3$, $\sigma 1$). Once the circle touches the stability criteria, failure occurs. If this failure happens within a short or longer time decides whether we experience an earthquake or fault creep. The proximity of the circle from the stability criteria indicates the stability of the system. A first approximation of the stress regime can be derived from Fig. 30, which shows the depth-dependent ratio of horizontal to vertical stresses.

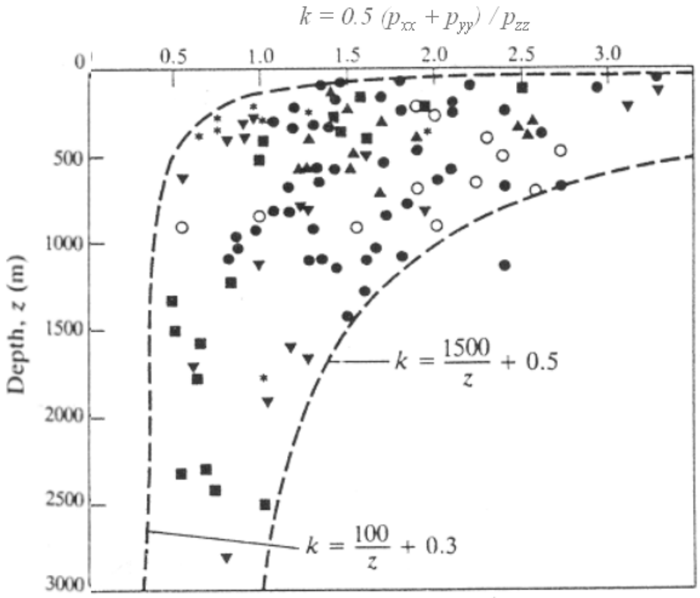

***Figure 30**. Depth versus the ratio of horizontal/vertical stress (Brady & Brown, 1985).*

A k-value (see Fig. 30) greater than 1 refers to a thrusting regime, whereas a ratio < 1 indicates a state of stress favouring normal faulting.

Seismic Event Size

Once the state of stress has been determined, the stability of a fault plane - and possible seismic events generated by slip along that fault plane - can estimated via the seismic moment (Aki & Richards, 1980), and subsequently its seismic magnitude:

$$Mo = A.D.G \qquad [17]$$

with

Mo... Seismic moment (Nm)
A... Area of slip (m^2)
D... Average displacement across the fault plane (m)
G... Shear modulus (N/m^2), usually 30 GPa

The fault plane (approximated by a circle of radius „r“), which was subjected to slip, can be estimated from the seismic moment (Brune, 1970, 1971):

$$r^3 = (7/16)\ Mo\ /\ \Delta\tau \qquad [18]$$

with $\Delta\tau$ being the shear stress drop, which is similar to the cohesion “So” of the fault (Ryder, 1988). Hence, the fault radius scales with the third power of the seismic moment Mo – and consequently the magnitude (Fig. 31), when using Hanks & Kanamori’s (1979) relation

$$M = (\log Mo - 9.1) / 1.5 \qquad [19]$$

This equation implies a shear stress drop of 1/10.000 of the shear modulus (usually 20–30 GPa), that is 2–3 MPa. Such values have been observed in practice (Scholz, 1990).

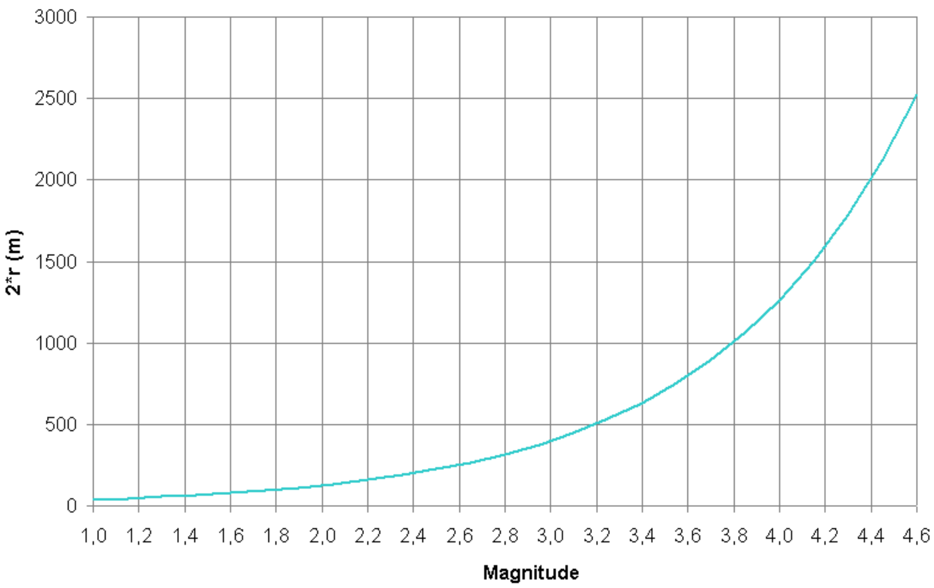

Figure 31. *Magnitude versus diameter of circular fault slip plane (= 2r).*

6.2 Case Studies

The most famous case of induced seismicity in this regard in Europe occurred in Basel during a hydro-fracking (well pressures in excess of 30 MPa) operation, which constitutes an Enhanced Geothermal System (EGS). The largest seismic event had a magnitude of M3.4, and some of which were strong enough to be noticed by the public across the City of Basel. Considering historical seismicity and the famous Basel-earthquake in 1356, the operation of the geothermal plant was then abandoned.

It took more than a year for the seismic activity to calm down (Fig. 32). Obviously, the water under high pressure utilized existing fault structures to propagate, thus lubricating these fault structures and triggering moderate earthquakes.

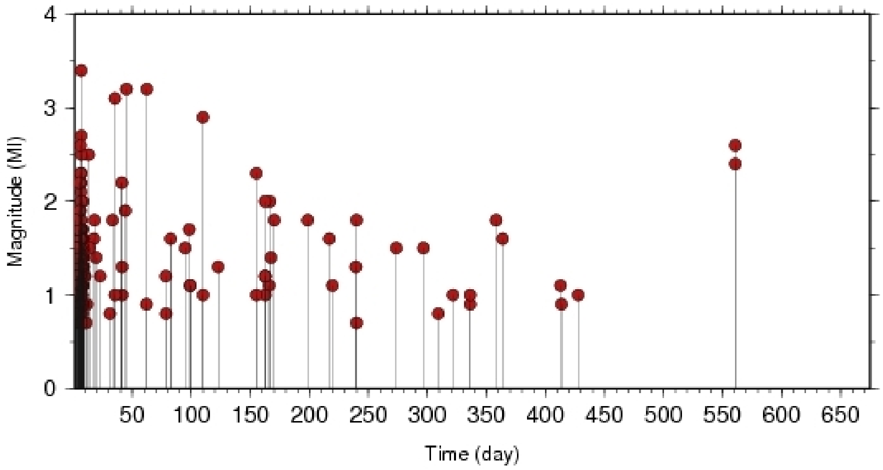

Figure 32. *Seismicity in Basel after stimulation in December 2006 (http://www.seismo.ethz.ch/basel/)*

Another example of geothermal associated seismicity is given in Table 7. These seismic events were not triggered due to enhanced borehole operations, but are genuinely related to the geothermal power plants near Munich in Germany. Some of these events were strong enough to be felt by the public.

Table 7. *List of associated seismic events (time = UTC) near Munich*

Nr.	Year	Month	Day	UTC	Lat.	Long.	Mag	Epicentre
1.	2008	02	10	22:49	48.04	11.63	2.5	Oberhaching
2.	2008	07	03	20:16	48.05	11.68	2.6	Oberhaching
3.	2008	07	21	00:53	48.08	11.66	2.2	Oberhaching
4.	2008	07	23	03:33	48.06	11.69	2.0	Oberhaching
5.	2008	10	19	05:48	48.23	11.50	1.8	Oberschleissheim
6.	2009	02	02	20:55	48.08	11.71	2.3	Oberhaching
7.	2009	02	02	21:27	48.08	11.72	1.9	Oberhaching
8.	2010	05	27	16:24	48.08	11.67	2.2	Oberhaching
9.	2011	08	23	21:34	48.27	11.41	1.2	Dachau
10.	2013	04	16	21:51	48.05	11.65	2.0	Oberhaching
11.	2013	04	16	22:15	48.03	11.63	1.6	Oberhaching
12.	2016	11	19	17:41	48.18	11.78	1.8	Erding
13.	2016	12	07	05:28	48.20	11.81	2.5	Erding
14.	2016	12	10	13:38	48.20	11.81	2.0	Erding
15.	2016	12	20	03:30	48.19	11.77	2.2	Erding
16.	2020	03	10	22:04	48.05	11.65	1.9	Oberhaching

6.3 Application to Laa/Pasohlávky Region

As there is no borehole information available from the planned site Pasohlávky in Czechia, we discuss here the potential of seismic events in the area of Laa an der Thaya (Fig. 33) in Austria.

The maximum depth of the boreholes reach from 2640 (Laa TH S1, re-injection) to 1448 m (Laa TH N1, production). Vertical stresses σ1, given an average density of the overburden of 2400 kg/m³, should then amount to 62 MPa at TH S1 and 34 MPa at TH N1 at the well bottom. The corresponding horizontal stresses would then amount to 19 MPa and 10 MPa, respectively. Admitting, this stresses depend also to a certain extent on the Poisson's ratios of the rocks in the geological Eggenburg/Eger and Jura units.

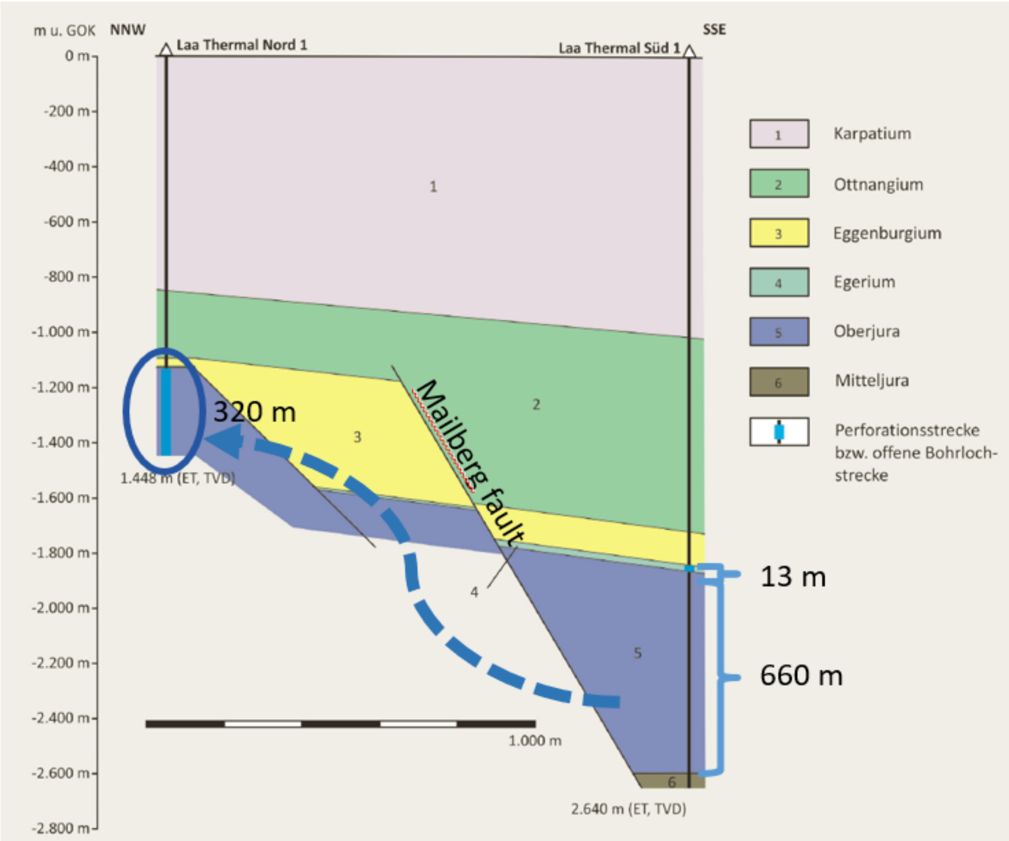

Figure 33. *Section of the Mailberg fault zone with both boreholes (Bottig, 2019)*

Given a fault plane which extends 850 m on dip, a seismic event of magnitude M3.4 (Fig. 31) would be possible, if the shear wave velocity "vs" amounts to 1800 m/s. Increasing "vs" to 3400 m/s would lead to an earthquake magnitude of M3.7.

The remaining questions is: Did the total displacement take place in numerous sudden jerks, or creep? The absence of any seismic activity during the operation of the thermal bath in Laa an der Thaya may serve as strong indicator, that fault displacements – if any (there is no evidence since the Badenian) – at the Mailberg fault are taking place in a creep-like fashion.

6.4 Simulation of Ground Motion from M3.0 Induced Earthquake

The U.S. Geological Survey (USGS) ShakeMap is a well-established tool used to portray the extent of potentially damaging ground shaking following an earthquake (Wald et at. 1999). ShakeMap is a seismologically based interpolation algorithm that combines observed data and seismological knowledge to produce maps of peak ground motion (PGM). The shaking is represented through maps of peak ground acceleration (PGA), peak-ground velocity (PGV), response spectral acceleration (SA), and ground-motion shaking intensity. The *instrumental intensity* values are derived from the conversion of PGM into intensity values (e.g. Wald et al. 1999A). Intensity can be defined as a classification of the strength of shaking at any place during an earthquake, in terms of its observed effects on buildings and human beings.

A ShakeMap earthquake scenario is simply a ShakeMap with an assumed magnitude and location and, optionally specified fault geometry. Ground motions are usually estimated using Ground Motion Prediction Equations (GMPEs) to compute peak ground motions. For our calculations we used the GMPE proposed by Atkinson and Boore (2006). In order to visualize the extent of ground shaking caused by a hypothetical earthquake in the area of interest, we created a ShakeMap scenario for an earthquake of M 3.0 on the Mailberg Fault near the city of Laa an der Thaya (Fig. 34). An earthquake of this magnitude in shallow depth would generate a ground shaking of intensity VI, which, in the EMS-98, is described as "Sightly damaging, for example, fine cracks in plaster and small pieces of plaster fall."

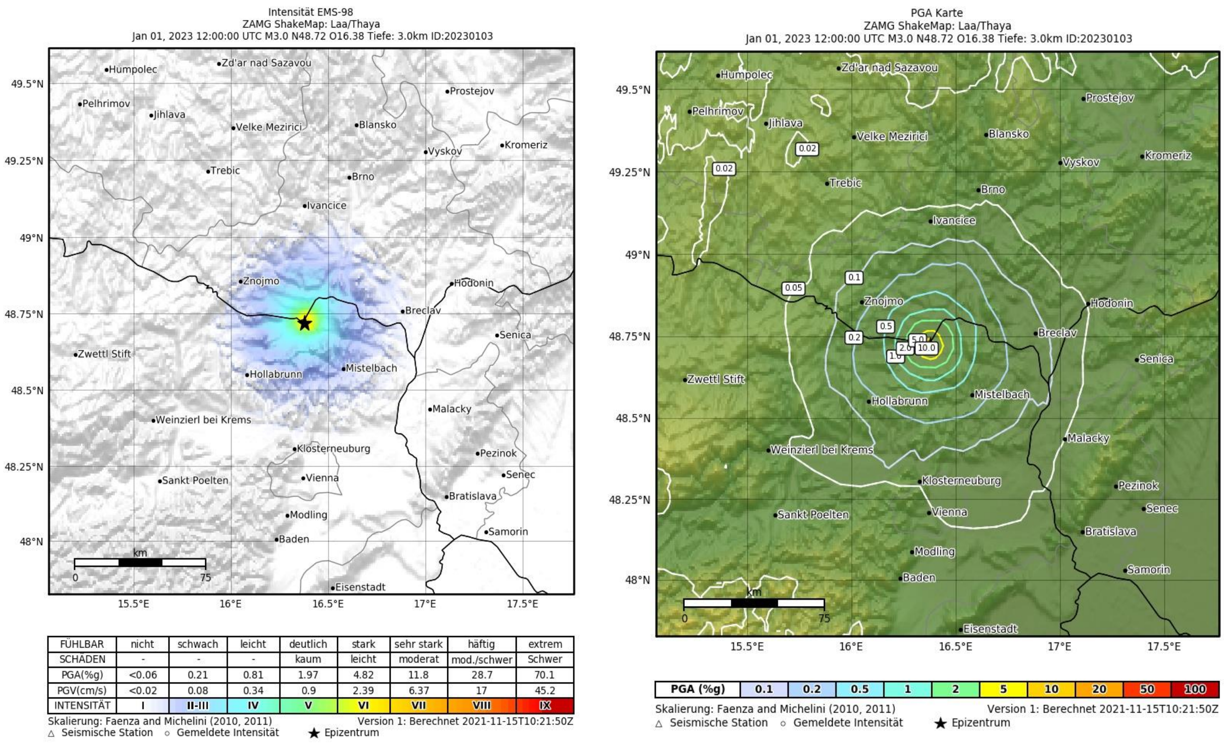

Figure 34. *Example of the ShakeMaps for intensity (left) and peak-ground-acceleration (right) for a hypothetical earthquake of M 3.0 on the Mailberg Fault near the city of Laa an der Thaya.*

7 Conclusions

Based on the revised archival macroseismic and instrumental observations and the results of a 38-month period of detailed monitoring by an enhanced network of stations, regional earthquake catalogues were created for the broad Laa/Pasohlávky area.

These catalogues provide unprecedentedly accurate knowledge on past and present seismicity in a wide cross-border area covering the southern part of the Bohemian Massif, the northern part of the Eastern Alps, most of the Vienna Basin and part of the Western Carpathians.

The rare major prehistoric earthquakes that have been recorded in the geological record so far are all Pleistocene and most likely related to major faults.

Very low local seismicity in the area of interest was quantified by the earthquake recurrence model which can serve as a baseline reference for comparing seismicity levels before and after the start of exploitation of thermal waters in the area of interest.

Seismic wave attenuation was quantified using models based on unprecedentedly rich local observations.

With the knowledge gained and based on the maximum magnitude estimated, ground shaking scenarios were modelled to show what peak ground motions can be expected in the event of a stronger induced earthquake.

The following cautions and recommendations are provided for case that intensive use of thermal waters is initiated:

- With a very low level of natural seismicity it is likely that virtually any detected earthquake – and definitely any felt earthquake – with epicentre in the Laa/Pasohlávky area may be considered anthropogenic
- Shallow weak earthquakes of magnitude M≈1 are likely to be felt by people within 10 km of the epicentre.
- Extreme cases of induced earthquakes with M≥3 at shallow depths could lead to shaking with an epicentral intensity of up to 6-7. Locally, ground motion can be amplified by sediments. Such earthquake may cause slight damage near epicentre and might be felt by people over an area of ~3000 km^2 which includes larger municipalities with population of >10000.
- Dramatic increase in seismicity with magnitudes in the upper part of the considered range is not expected for low injection/extraction rates. However, in case of larger exploitation the local seismicity response must be monitored and measures should be adopted to prevent the increase.
- The need to regulate production rates based on the observed current seismicity rates must be taken into account.

8 References

Aki, K., 1965: Maximum likelihood estimate of b in the formula log n= a-bm and its confidence limits. Bull. Earthq. Res. Inst., Tokyo Univ., vol. 43, pp. 237-239.

Aki, K. & Richards, P.G. 1980: Quantitative Seismology - Theory and Methods. Freeman and Company, San Francisco.

Atkinson, G.M., 2004: Empirical attenuation of ground motion spectral amplitudes in southeastern Canada and the northeastern United States, Bull. Seismol. Soc. Am. 94, 1079–1095.

Atkinson, G., and Boore, D., 2006: Ground motion prediction equations for earthquakes in eastern North America, Bull. Seismol. Soc. Am. 96, 2181–2205.

Atkinson, G.M. and Kaka S.I., 2007: Relationships between Felt Intensity and Instrumental Ground Motion in the Central United States and California. Bulletin of the Seismological Society of America 97, 2, 497–510, doi: 10.1785/0120060154

Atkinson, G.M. and Wald, D.J., 2007: "Did You Feel It?" Intensity Data: A Surprisingly Good Measure of Earthquake Ground Motion. Seismological Research Letters 78 (3), 362-368.

Atkinson, G.M., Warden, C.B. and Wald, D.J., 2014: Intensity Prediction Equations for North America. Bulletin of the Seismological Society of America 104 (6), 3084–3093. doi: 10.1785/0120140178

Arroucau, P., Mocquet, A., & Vacher, P., 2006: Macroseismic intensity attenuation for Metropolitan France: importance of the epicentral intensity.

Bakun, W.H. and Scotti, O., 2006: Regional intensity attenuation models for France and the estimation of magnitude and location of historical earthquakes. Geophys. J. Int. 164, 596–610. doi: 10.1111/j.1365-246X.2005.02808.x

Boore, D. 2003: Simulation of ground motion using the stochastic method, Pure Appl. Geophys. 160, 636–676.

Bottig, M., 2019: Presentation at the first Project Team Meeting (M.1.2). 10 slides.

Brady, B.H.G. & Brown, E.T., 1985: Rock Mechanics for Underground Mining, George Allen & Unwin Publishers.

Brune, J., 1970, 1971: Tectonic stress and the spectra of seismic shear waves from earthquakes. J.Geophys.Res. 75, 1970, 4997–5009 (correction in J.Geophys.Res. 76, 1971, 5002).

Burger, R., Somerville P., Barker J., Herrmann R., and Helmberger D., 1987: The effect of crustal structure on strong ground motion attenuation relations in eastern North America, Bull. Seismol. Soc. Am. 77, 420–439.

Caprio, M., Tarigan, B., Worden, C.B., Wiemer, S., Wald, D.J., 2015: Ground motion to intensity conversion equations (GMICEs): a global relationship and evaluation of regional dependency. Bull Seismol Soc Am 105(3):1476–90.

Davis, S.D. & Pennington, W.D., 1989: Induced seismic deformation in the Cogdell Oil Field of West Texas. Bull.Seism.Soc.Am., Vol.79, 1477–1491.

Decker, K., 1999: Tektonische Auswertung integrierter geologischer, geophysikalischer, morphologischer und strukturgeologischer Daten. (Projekt N-C-036/F/98 Geogenes Naturraumpotential Horn-Hollabrunn). Ms. Geol. B.-A., Wien.

Dlabač, M. et al., 1972: Vysvětlující text k základní geologické mapě 1:25 000 M-33-117-C-b Jaroslavice. ÚÚG, Brno, 168 s.

Dornič, J. et al., 1985: Vysvětlivky k základní geologické mapě ČSSR 1:25 000; 34-114 Prosiměřice. ÚÚG, Praha, 50 s.

Drimmel, J. & Trapp, E., 1975: Das Starkbeben am 29. Januar 1967 in Molln, Oberösterreich. – Mitt. d. Erdbebenkomm. Akad. Wiss., N.F. 76, 1–45, Wien.

Drimmel, J., 1980: Rezente Seismizität und Seismotektonik des Ostalpenraumes. – In: Oberhauser, R. (Ed.): Der Geologische Aufbau Österreichs, 506–527, Wien.

Drimmel, J., 1990 Explanation of the anomalous energy propagation of east Alpine transversal quakes. In: Minaříková, D. and Lobitzer, H. (Eds.) 1990 Thirty years of geological cooperation between Austria and Czechoslovakia. 1990, 32-37. Ústřední ústav geologický, Prague.

Edwards, B., Fäh, D., and Giardini, D., 2011: Attenuation of seismic shear wave energy in Switzerland, Geophys. J. Int. 185, 967–984.

Faenza L, Michelini A., 2010 Regression analysis of MCS intensity and ground motion parameters in Italy and its application in ShakeMap. Geophys J Int 180:1138–52.

Galli, P., 2000: New empirical relationships between magnitude and distance for liquefaction. Tectonophysics 324:169–187.

Gardner, J. and Knopoff, L., 1974: Is the sequence of earthquakes in southern california, with aftershocks removed, poissonian? Bulletin of the seismological society of America , vol. 64, no. 5, pp. 1363-1367.

Granado, P., Thöny, W., Carrera, N., Gratzer, O., Strauss, P., Muñoz, J.A., 2016: Basement-involved reactivation in fold-and-thrust belts: the Alpine-Carpathian Junction (Austria). Geological Magazine 153 (5-6), 1110-1135, doi: 10.1017/S0016756816000066.

Gutenberg, B. and Richter, C. F., 1944: Frequency of earthquakes in california. Bulletin of the Seismological society of America , vol. 34, no. 4, pp. 185-188.

Hammerl, Ch. & Lenhardt, W.A., 2013: Erdbeben in Niederösterreich von 1000 bis 2009 n. Chr. – Abh. Geol. B.-A., 67, Wien, 297 S.

Hammerl, Ch., Pazdírková, J., Rodler, F.-A., Krumlová, H., 2021: Seismicity before 2018. Technical report T1.2.1, Interreg Project ATCZ167 „Hydrothermal Potential of the Laa an der Thaya / Pasohlávky area“ (HTPO).

Hanks, T.C. & Kanamori, H. 1979. A moment-magnitude scale. J.Geoph.Res. 84, 2348–2350.

Hintersberger, E., Decker, K., Lomax, J. and Lüthgens, Ch., 2018: Implications from palaeoseismological investigations at the Markgrafneusiedl Fault (Vienna Basin, Austria) for seismic hazard assessment. Nat. Hazards Earth Syst. Sci., 18, 531–553. https://doi.org/10.5194/nhess-18-531-2018

House, L.S. & Flores, R., 2002: Seismological Studies of a Fluid Injection in Sedimentary Rocks, East Texas. Pure appl. geophys. (2002), 371–401.

Isaba, M. D. P. P., Weginger, S., Apoloner, M. T., Jia, Y., Hausmann, H., Meurers, R., & Lenhardt, W., 2020: *Intensity Prediction Equation for Austria: Applications and analysis* (No. EGU2020-7683). Copernicus Meetings.

Ishimoto, M., 1936: Observations of earthquakes registered with the micro-seismograph constructed recently. Bull. Earthquake Res. Inst. Univ. Tokyo, vol. 17, pp. 443-478.

Jaeger, J.C., Cook, N.G.W. & Zimmermann, R.W., 2007: Fundamentals of Rock Mechanics. 4th edition. Blackwell Publishing Ltd.

Keefer, D.K., 1984: Landslides caused by earthquakes. Geological Society of America Bulletin 95, 406 – 421.

Kövesligethy, R., 1907: Seismischer Stärkegrad und Intesität der Beben. Gerlands Beiträge zur Geophysik, Bd 8, 22-29.

Krischer, L., Megies, T., Barsch, R., Beyreuther, M., Lecocq, T., Caudron, C., and Wassermann, J., 2015: Obspy: A bridge for seismology into the scientific python ecosystem. Computational Science & Discovery , vol. 8, no. 1, p. 014003.

Lenhardt, W.A., 1998: Erdbeben der vierten Art. Bautechnik 75, Heft 10, 781–791.

McGarr, A., 1991: On a possible connection between three major earthquakes in California and oil production. Bull.Seism.Soc.Am., Vol.81, No.3, 948–970.

McGarr, A. (ed.), 1993: Induced seismicity. Birkhäuser Verlag, reprint from PAGEOPH, Vol. 139 (1992), No.3/4.

McGarr, A. & Simpson, D., 1997: Keynote lecture: A broad look at induced seismicity. Proc. of 4th Int. Symp. on 'Rockbursts and Seismicity in Mines', Balkema, 385–396.

Mignan, A., and Woessner, J., 2012: Estimating the magnitude of completeness for earthquake catalogs. Community Online Resource for Statistical Seismicity Analysis, pp. 1-45.

Möllhoff, M., Bean, C. J. and Baptie, B. J., 2019: Sn-cast: seismic network capability assessment software tool for regional networks-examples from ireland. Journal of Seismology, vol. 23, no. 3, pp. 493-504.

Nehyba, S., Opletal, V., Chroustová, K., Pasternáková, B., Kuchovský, T., Říčka, A., Bottig, M., 2021: Structural geological - hydrogeological map series of the thermal water bearing formations in the region, Output T1.1.1 of the project AT-CZ167 (HTPO). https://www.at-cz.eu/cz/ibox/po-2-zivotni-prostredi-a-zdroje/atcz167_htpo/dokumenty

Obermeier, S.F., Pond, E.C., Olsen, S.M. with contributions by Green, R.A., Mitchell, J.K., and Stark,T.D. 2001: Paleoliquefaction studies in continental settings: geologic and geotechnical factors in interpretations and back-analysis. U.S. Geological Survey Open-File Report 01-029.

Otáhalová M. and Melichar R. 2007: Tectonics of Neogenous rocks from the Southern part of Carpathian Foredeep in the Hevlín surroundings. Geologické výzkumy na Moravě a ve Slezsku, 2017, 28-30. (in Czech)

Pasolini, C., Gasperini, P., Albarello, D., Lolli, B., & D'Amico, V., 2008: The attenuation of seismic intensity in Italy, part I: Theoretical and empirical backgrounds. *Bulletin of the Seismological Society of America*, *98*(2), 682-691.

Pezeshk S., Zandieh A., and Tavakoli B., 2011: Hybrid Empirical Ground-Motion Prediction Equations for Eastern North America Using NGA Models and Updated Seismological Parameters. Bulletin of the Seismological Society of America 101, 4, 1859–1870. doi: 10.1785/0120100144

Peterson, J. et al., 1993: Observations and modeling of seismic background noise.

Procházková, D., 1982: Attenuation of macroseismic effects of earthquakes. Travaux Géophysiques 30, 569, 47-93. Prague

Procházková, D. and Kárník, V. (eds.), 1978: Atlas of Isoseismal Maps. Central and Eastern Europe. Geophysical Institute of the Czechoslovak Academy of Science, Prague, 135 pp.

Quigley, MC, Hughes, MW, Bradley, BA, van Ballegooy, S, Reid, C., Morgenroth, J., Horton, T., Duffy, B., Pettinga, JR., 2016: The 2010–2011 Canterbury Earthquake Sequence: Environmental effects, seismic triggering thresholds and geologic legacy, Tectonophysics 672–673, 228-274. doi.org/10.1016/j.tecto.2016.01.044

Rietbrock, A., Strasser, F., and Edwards, B., 2013: A stochastic earthquake ground-motion prediction model for the United Kingdom, Bull Seismol. Soc. Am. 103, no. 1, 57–77.

Rodler, F.-A., Krumlová, H., Pazdírková, J., 2021: Earthquake catalogue 01/2018 - 09/2021. Technical report T1.3.1, Interreg Project ATCZ167 „Hydrothermal Potential of the Laa an der Thaya / Pasohlávky area“ (HTPO).

Roštínský, P., Pospíšil, L., Švábenský, O. 2013: Recent geodynamic and geomorphological analyses of the Diendorf–Čebín Tectonic Zone, Czech Republic. Tectonophysics, 599, 45–66.

Roštínský, P., Pospíšil, L., Švábenský, O., Kašing, M., Nováková, E., 2020: Risk faults in stable crust of the eastern Bohemian Massif identified by integrating GNSS, levelling, geological, geomorphological and geophysical data. Tectonophysics 785, 228427.

Rydelek, P. A. and Sacks, I.S., 1989: Testing the completeness of earthquake catalogues and the hypothesis of self-similarity. Nature , vol. 337, no. 6204, pp. 251-253.

Ryder, J.A., 1988: Excess shear stress in the assessment of geologically hazardous situations. J.S.Afr.Inst.Min.Metall., Vol.88, pages 27–39.

Scherbaum, F. and Stoll D., 1983: Source parameters and scaling laws of the 1978 Swabian Jura (southwest Germany) aftershocks. Bull. Seismol. Soc. Amer., 73, 1321-1343.

Schippkus, S., Hausmann, H., Duputel, Z., Bokelmann, G., AlpArray Working Group, 2019: The Alland earthquake sequence in Eastern Austria: Shedding light on tectonic stress geometry in a key area of seismic hazard. Austrian Journal of Earth Sciences 112/2, 182-194. DOI: 10.17738/ajes.2019.0010

Scholz, C.H., 1990: The mechanics of earthquakes and faulting. University Press, Cambridge, 471 pp

Shearer, P. M. and Stark, P. B., 2012: Global risk of big earthquakes has not recently increased. Proceedings of the National Academy of Sciences, vol. 109, no. 3, pp. 717-721.

Shebalin, N., 1958: Correlation between earthquake magnitude and intensity. Studia Geophysica et Geodaetica, vol. 2, p. 86.

Špaček, P., Valenta, J., Tábořík, P., Ambrož, V., Urban, M., Štěpančíková, P. 2017: Fault slip versus slope deformations: Experience from paleoseismic trenches in the region with low slip-rate faults and strong

Pleistocene periglacial mass wasting (Bohemian Massif). Quaternary International 451, 56-73. doi: 10.1016/j.quaint.2017.05.006

Špaček, P., Prachař, I., Roštínský, P., 2018: Summary report on the Diendorf-Boskovice fault zone activity assessment. Project ČEZ, a.s. Dukovany Nuclear Power Plant - Paleoseismological survey of the NPP EDU site. Unpublished report of Inst. Physics of the Earth, Masaryk University. Brno. (In Czech)

Špaček, P., Zacherle, P., Bokelman, G., Schippkus, S., Meurers, R., Pazdírková, J. and AlpArray Working Group, 2021: Crustal shear wave blockage in and around the Eastern Alps from the 2016 Alland earthquake. EGU General Assembly 2021, doi.org/10.5194/egusphere-egu21-8183

Sponheuer, W., 1960. Methodology for the identification of focal depth in macroseismic studies. Freiberger Forschungshefte, 88, p. 117.

Stromeyer, D., & Grünthal, G., 2009: Attenuation relationship of macroseismic intensities in Central Europe. *Bulletin of the Seismological Society of America*, *99*(2A), 554-565.

Talebi, Sh. (ed.), 1998: Seismicity caused by mines, fluid injections, reservoirs, and oil extraction. Pageoph, Vol. 153, No. 1, 233 pp.

Talwani, P. & Acree, S., 1985: Pore-pressure diffusion and the mechanism of reservoir-induced seismicity. Pure and Appl. Geophys., Vol.122, 947–965.

Trifu, C. (ed.) 2002: The mechanism of induced seismicity. Pageoph, Vol. 159, No. 1–3, Special Issue, 617 pp.

Tselentis, G-A, Danciu, L., 2008: Empirical relationships between modified Mercalli intensity and engineering ground-motion parameters in Greece. Bull Seismol Soc Am 98(4):1863–75.

Utsu, T., Ogata, Y., Matsu'ura, R.S., 1995: The centenary of the omori formula for a decay law of aftershock activity. Journal of Physics of the Earth , vol. 43, no. 1, pp. 1-33.

Wagner, L.R., 1998: Tectono-stratigraphy in the Molasse Foredeep of Salzburg, Upper and Lower Austria. In: Cenozoic Foreland Basins of Western Europe (Eds. A. Mascle, C. Puigdefàbregas, H.P. Luterbacher & M. Fernàndez). Geological Society, London, Special Publication 134, pp. 339–369.

Wald, D. J. , Quitoriano, V., Heaton, T. H., Kanamori, H., 1999 (B): Relationships between peak ground acceleration, peak ground velocity, and modified mercalli intensity in california. Earthquake spectra, vol. 15, no. 3, pp. 557-564.

Wald, D. J. , Quitoriano, V., Heaton, T. H., Kanamori, H., Scrivner, C. W. and Worden, C. B., 1999 (A): Trinet "shakemaps": Rapid generation of peak ground motion and intensity maps for earthquakes in southern california. Earthquake Spectra, vol. 15, no. 3, pp. 537-555.

Woessner, J. and Wiemer, S., 2005: Assessing the quality of earthquake catalogues: Estimating the magnitude of completeness and its uncertainty. Bulletin of the Seismological Society of America, vol. 95, no. 2, pp. 684-698.

Zanini, M.A., Hofera, L., Faleschinia, F., 2019: Reversible ground motion-to-intensity conversion equations based on the EMS-98 scale. Engineering structures 180, 310-320

Zeman, A. 1974: Současný stav výzkumu pleistocenních fluviálních sedimentů v Dyjsko-svrateckém úvalu a jejich problematika. Stud. geogr., 36, 41–75.